iScience

CellPress
OPEN ACCESS

Article

Diverse epistatic effects in barley-powdery mildew interactions localize to host chromosome hotspots

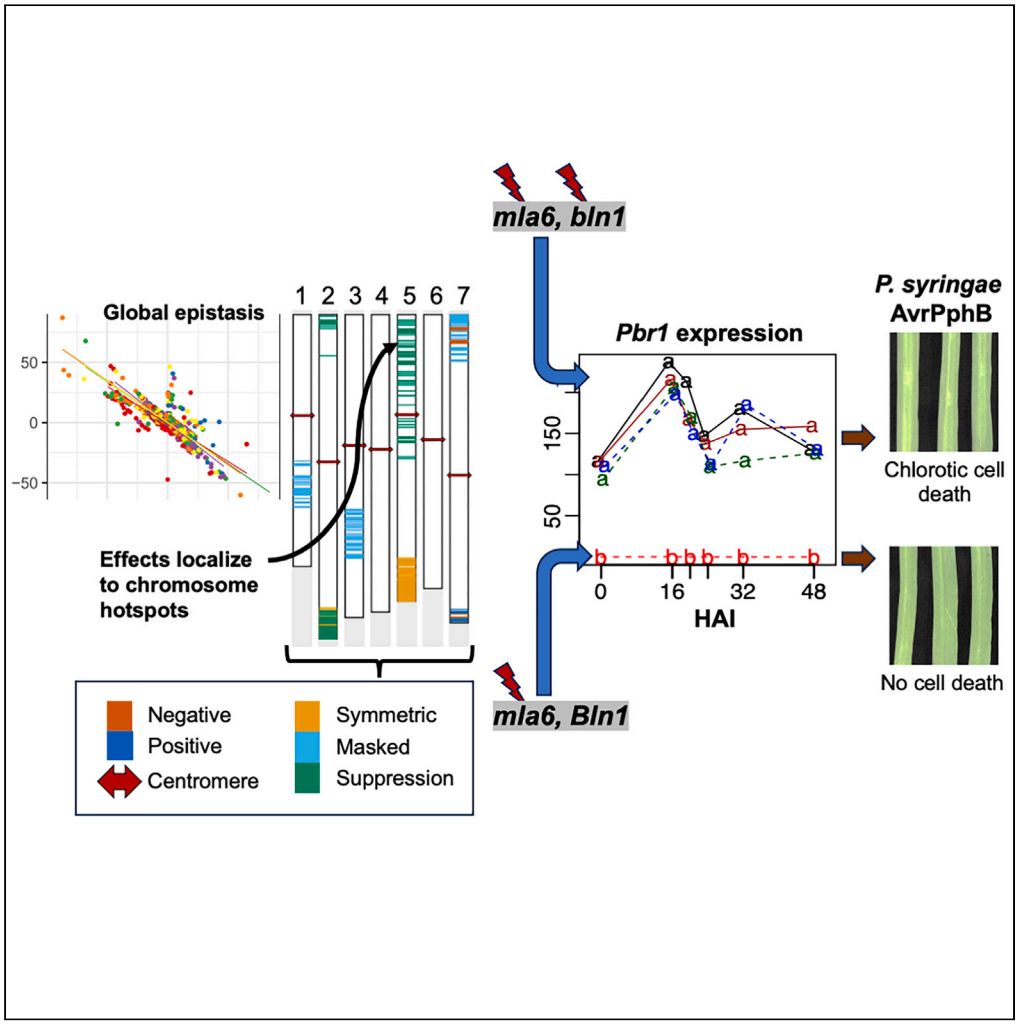

Valeria Velásquez-Zapata, Schuyler Smith, Priyanka Surana, Antony V.E. Chapman, Namrata Jaiswal, Matthew Helm, Roger P. Wise

Roger.Wise@usda.gov

Highlights

One-hundred fifteen NLRs localize to host chromosome, epistasis effect hotspots

Differential immunity to AvrPphB associated with suppression epistasis of *HvPbr1*

Masked epistasis influences *bln1*-coupled response to powdery mildew

Nine WGCNA co-expression modules link *Blumeria* effectors and fungal development

Velásquez-Zapata et al., iScience *27*, 111013
October 18, 2024 Published by Elsevier Inc.
https://doi.org/10.1016/j.isci.2024.111013

iScience

CellPress
OPEN ACCESS

Article

Diverse epistatic effects in barley-powdery mildew interactions localize to host chromosome hotspots

Valeria Velásquez-Zapata,[1,2,8] Schuyler Smith,[2] Priyanka Surana,[3] Antony V.E. Chapman,[4,5] Namrata Jaiswal,[6] Matthew Helm,[6] and Roger P. Wise[1,2,4,7,9,*]

SUMMARY

Barley *Mildew locus a* (*Mla*) encodes a multi-allelic series of nucleotide-binding leucine-rich repeat (NLR) receptors that specify recognition to diverse cereal diseases. We exploited time-course transcriptome dynamics of barley and derived immune mutants infected with the powdery mildew fungus, *Blumeria hordei* (*Bh*), to infer gene effects governed by *Mla6* and two other loci significant to disease development, *Blufensin1* (*Bln1*), and *Required for Mla6 resistance3* (*rar3* = *Sgt1*$_{\Delta KL308\text{-}309}$). Interactions of *Mla6* and *Bln1* resulted in diverse epistatic effects on the *Bh*-induced barley transcriptome, differential immunity to *Pseudomonas syringae* expressing the effector protease AvrPphB, and reaction to *Bh*. From a total of 468 barley NLRs, 115 were grouped under different gene effect models; genes classified under these models localized to host chromosome hotspots. The corresponding *Bh* infection transcriptome was classified into nine co-expressed modules, linking differential expression with pathogen structures, signifying that disease is regulated by an inter-organismal network that diversifies the response.

INTRODUCTION

Plant pathogenic fungi are among the greatest deterrents to crop production worldwide.[1–3] Obligate biotrophs, such as mildews and rusts, are unable to survive autonomously, and as such, present an ideal opportunity to examine interdependent gene regulation between disease agents and their hosts.[4,5] Yet, much remains to be discovered regarding the temporal and spatial control of these interconnected processes.[6,7] We have used the association between the powdery mildew fungus, *Blumeria hordei* (*Bh*), and its diploid host plant, barley (*Hordeum vulgare* L.) to tease apart the complex genetics underlying their interaction. Subsequent to the germination of haploid conidia and appressorial penetration of the host cuticle, *Bh* secretes effector proteins into epidermal cells via haustorial feeding structures.[8,9] These effectors allow the fungus to evade host immune responses and acquire nutrients to support colonization.[10–17] Disease is blocked by immune receptors encoded by host resistance (*R*) genes,[18] designated by the prefix *Ml* (for mildew resistance[19–24]).

Intracellular nucleotide-binding leucine-rich repeat (NLR) immune receptors are encoded by some of the largest gene families in plants, with 5408 in the pan-genome of rice,[25] up to 7780 in the pan-NLRome of wheat,[26,27] 468 in barley,[28] and 265 in Arabidopsis.[29,30] These often occur in clusters throughout their respective genomes,[31,32] and once activated and translated, interact directly or indirectly with effector proteins secreted by pathogens.[18,33] The barley MLA (NLR-type) immune receptor family and its orthologs impart recognition to many cereal diseases, including powdery mildew, stem- and stripe rust, rice blast, and spot blotch.[34–41] In some cases, the identical MLA host protein determines recognition specificity to effectors from evolutionary diverged pathogens, for example, the adapted ascomycete *Bh* vs. the non-adapted (stripe rust) basidiomycete, *Puccinia graminis striformis*,[39] *Bh* and *Magnaporthe oryzae*, the causal agent of rice blast,[40] or *Bh* and the necrotrophic spot blotch pathogen, *Cochliobolus sativus*.[41]

To facilitate their function, host NLR immune receptors are often stabilized by additional proteins, for example, heat shock protein 90 (HSP90), required for *Mla12* resistance1 (RAR1), and suppressor of the G2 allele of SKP1 (SGT1)[21–23,42–44] as well as interacting with and activating each other.[18,29,45–48] On the pathogen side, coding sequences (CDS) for 534 candidate secreted effector proteins (CSEPs) have been

[1]Program in Bioinformatics & Computational Biology, Iowa State University, Ames, IA 50011, USA
[2]Department of Plant Pathology, Entomology, and Microbiology, Iowa State University, Ames, IA 50011, USA
[3]Informatics Infrastructure Team, Tree of Life Programme, Wellcome Sanger Institute, Hinxton, Cambridgeshire CB10 1SA, UK
[4]Interdepartmental Genetics & Genomics, Iowa State University, Ames, IA 50011, USA
[5]Phytoform Labs, Rothamsted Research, Harpenden AL5 2JQ, UK
[6]USDA-Agricultural Research Service, Crop Production and Pest Control Research Unit, West Lafayette, IN 47907, USA
[7]USDA-Agricultural Research Service, Corn Insects and Crop Genetics Research Unit, Ames, IA 50011, USA
[8]Present address: GreenLight Biosciences, Inc. Research Triangle Park, NC 27709
[9]Lead contact
*Correspondence: Roger.Wise@usda.gov
https://doi.org/10.1016/j.isci.2024.111013

identified from 893 secreted proteins encoded in the *Bh* genome.[14,49–52] A small subset of these CSEPs have been functionally characterized by the identification of their host targets, cellular localization, and/or gene silencing.[53–60]

Metatranscriptomes between host and pathogen can be used as a testing model to evaluate the cellular response of each organism and its genetic effects. If data from both progenitor and isogenic mutants are available, we reasoned that different gene effect models could explain the types of interactions between the mutated genes. Of these, one of the most utilized involves the estimation of epistasis, where gene effects are classified as additive or the product of gene interaction(s).[61,62] When single mutants of two genes are associated with a phenotype whose sum differs from the double mutant, this non-additivity indicates that epistasis is present (the two genes interact genetically). In this regard, RNA sequencing (RNA-Seq) can be used as a proxy for gene expression as a quantitative phenotype to perform gene effect analyses.[63] Gene expression is also heritable and linked to phenotypic variation at the microscopic and macroscopic levels.[64]

In this report, we used a dynamic transcriptome collected from the interaction between CI 16151 barley and a set of derived isogenic mutants infected with *Bh* to explore genetic effects governed by the NLR-type *R*-gene, *Mla6*, and two additional genes involved in host immunity, *Required for Mla6 resistance 3* (*Rar3;* identified as *Sgt1*)[43] and *Blufensin1* (*Bln1*).[65–67] Two epistasis models were inferred in the host; and in parallel, temporally associated co-expression modules were used to investigate the effects of the host environment on the pathogen. Genomic location is proposed as a possible mechanism of host gene effects by associating chromosome hotspots with the different genetic effect models. Results from this analysis point to a large perturbation network of host and pathogen arsenals under different genetic mechanisms that diversify expression patterns and increase the robustness of the response.

RESULTS

Barley-*Blumeria hordei* transcriptome dynamics enable the dissection of genetic interactions among *Mla6*, *Bln1*, and *Sgt1*

Here, we discuss how to model a host-pathogen metatranscriptome. Two main components are presented, the first regarding the genetics of the barley host, and the second, how *Blumeria hordei* (*Bh*) responds to the host environment through co-expression networks. Our panel of barley wildtype and isogenic immune mutants enabled us to define gene effect models for the *Mla6* NLR gene, which confers resistance to *Bh* isolates that secrete the AVR_{A6} effector; *Bln1*, an *R*-gene independent regulator of immunity[65–67]; and *Sgt1*, which is required for *Mla6*-mediated hypersensitive response and generation of H_2O_2.[43] As shown in Figure 1A and Figure S1, five genotypes were included in the design. The wild-type progenitor, CI 16151, contains the *Mla6* NLR gene, the susceptible *mla6*-m18982 mutant contains 168 single-nucleotide polymorphisms (SNPs), and 2 x 3-nucleotide indels in the *Mla6* coding sequence, resulting in 85 amino acid changes (Figures S2A–S2C). The resistant *bln1* mutant, *bln1*-m19089, contains a deletion of the gene (Figures S2D and S2E) and exhibits enhanced defense to compatible *Bh* isolates. The susceptible double mutant, (*mla6+bln1*)-m19028, contains both the *bln1* and *mla6* variants. Lastly, the susceptible *rar3*-m11526 mutant contains an in-frame Lys-Leu deletion in the SGS domain of the co-chaperone SGT1, which interacts physically with MLA.[21,43,44]

First leaf seedlings inoculated with fresh *Bh* conidiospores were sampled at 0, 16, 20, 24, 32, and 48 h after inoculation (HAI), covering *Bh* appressorium formation (0–16 HAI), penetration of epidermal cells (16–20 HAI), and development of haustorial feeding structures (24–48 HAI). Bulk RNA-Seq reads from both barley and *Bh* were processed, and transcript counts were analyzed to characterize gene expression (see STAR Methods). As shown in Figure 1B, a principal component analysis (PCA) was performed over the complete transcriptome and then plotted by timepoint to facilitate visualization. This analysis indicated that samples clustered by timepoint and genotype. The initial time point (0 HAI) is separated from the rest in the PC1 axis, which comprises 43% of the variance. The PC2 component contained 16% of the variance. When the PCA was separated by barley and *Bh* (Figure S3) we could observe that the *Bh* dataset is divided by disease phenotype, a pattern that is reinforced at later time points.

Differentially expressed genes (DEGs) were identified per timepoint taking as reference the wild-type progenitor CI 16151 and comparing across mutant genotypes (Table S1). As illustrated in Figure 1C, all susceptible mutants showed a peak in the number of barley DEGs at *Bh* penetration (20 HAI), with the (*mla6+bln1*)-m19028 double mutant exhibiting the highest number of DE genes. In contrast, the resistant *bln1*-m19089 mutant, had a low number of DEGs across the time course, without a peak as seen in the susceptible mutants. We also observed a considerable number of DEGs at 0 HAI, which could be due to low gene counts that were artificially inflated in the normalization process. We also expect that some of these DEGs can be explained by instantaneous transcriptional responses to *Bh* inoculation. This is reminiscent of the rapid response observed in barley-stem rust interactions. The RPG1 resistance protein is phosphorylated and degraded in response to avirulent, but not virulent isolates of *Puccinia graminis* f. sp. *tritici*,[68] as early as within 5 min after contact, and this is due to the action of two effectors that act cooperatively with RPG1 before haustoria formation.[69] Thus, depending on the particular interaction, it appears that some genes are dynamically expressed very early, and some act later.

Bh displayed different expression patterns from those found in the host. Most *Bh* DEGs were associated with the development of haustoria (32 and 48 HAI), starting with almost no DEGs at the penetration of barley epidermal cells (16 HAI) and gradually increasing over time. We also observed that the number of *Bh* DEGs in the resistant *bln1*-m19089 mutant were almost non-existent across the time course. These observations indicate that the host environment perceived by *Bh* and specifically the plant disease phenotype is the main determinant of *Bh* gene expression. At 0 HAI we also observed a high number of DEGs with *Bh* as compared to barley. Note here that there is a massive difference in sample abundance between the host and pathogen, and this could bias the effect of low read count inflation in the *Bh* analysis. Also, as an obligate biotroph, it could be possible that *Bh* is predisposed to interacting with its host, and that this is revealed in the susceptible *mla6+bln1* genotype.

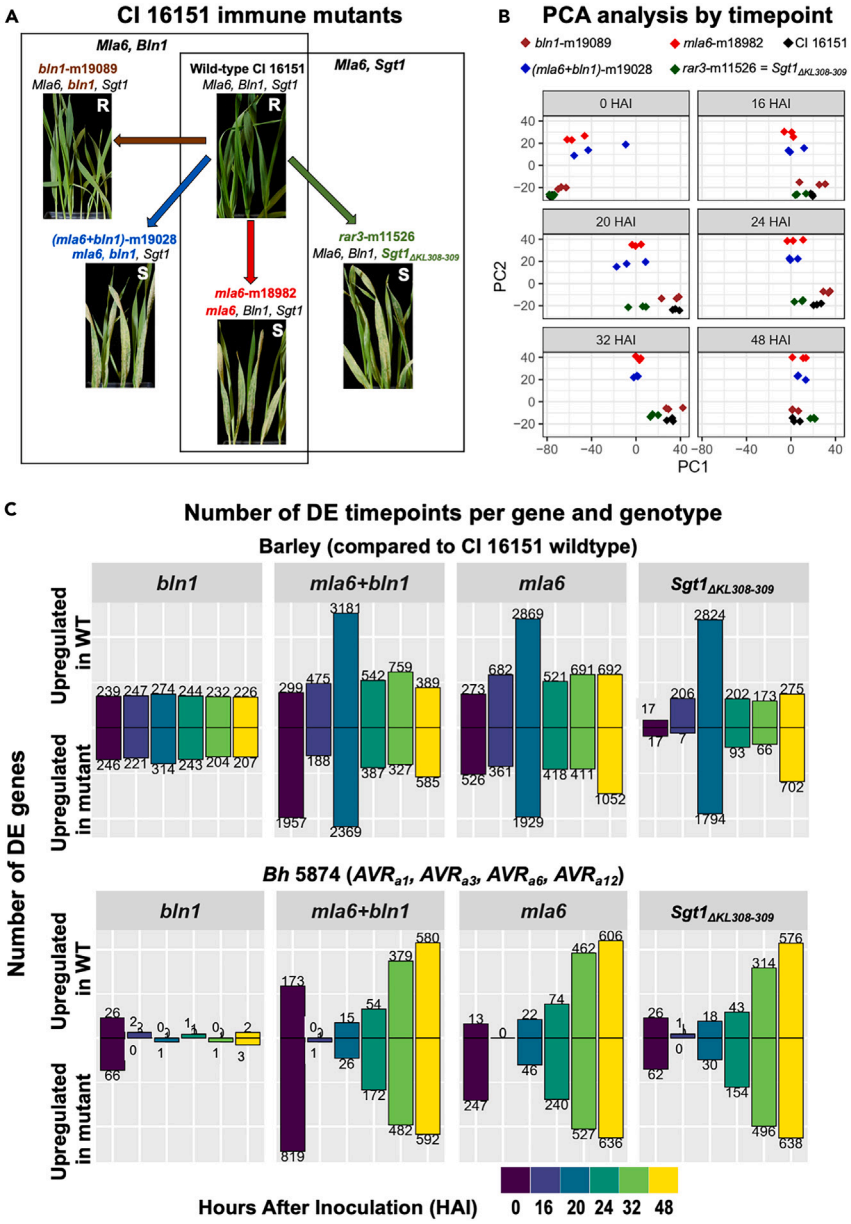

Figure 1. A dynamic barley-*Bh* transcriptome of immune mutants

(A) Wild-type progenitor CI 16151, carrying the *Mla6* gene conferring resistance to AVR_{a6} *Bh* isolates, and four isogenic mutants derived by fast-neutron mutagenesis of the CI 16151 progenitor were used to investigate the effects of the functionally connected, but physically unlinked, *Mla6*, *Bln1* and *Sgt1*. Lineages used in each of the *Mla6*, *Bln1* and the *Mla6*, *Sgt1* models are boxed.

(B) PCA analysis of the RNA-Seq samples obtained from the immune mutant panel, colored by genotype, and separated by timepoint.

(C) Number of DE genes per timepoint in barley or *Bh*, separated by mutant and foldchange (overexpressed in wild-type or in the mutant). Significance cutoffs for DE genes were determined at adjusted *p*-values of 0.001 (barley) and 0.003 (*Bh*).

Global and gene-wise epistasis indicate that *Mla6* and *Bln1* interact genetically

Using gene expression as a phenotype, we calculated the genome-wide epistatic effects of *Mla6* and *Bln1*, using a global index defined by Angeles-Albores and colleagues.[63] Predicted additive effects of these genes were calculated, separating the data for each timepoint.

Observed genetic effects per timepoint were compared to the predicted additive effects (see STAR Methods). Figure 2A shows the genome-wide comparison between the predicted additive and the deviation from the observed genetic effects of *Mla6* and *Bln1*, for each timepoint. From this plot, we can estimate the global epistasis index as the slope of the line. According to this model, a slope of zero indicates no epistasis, and deviations from zero indicate global epistasis. Subsequently, we calculated the range at each timepoint,

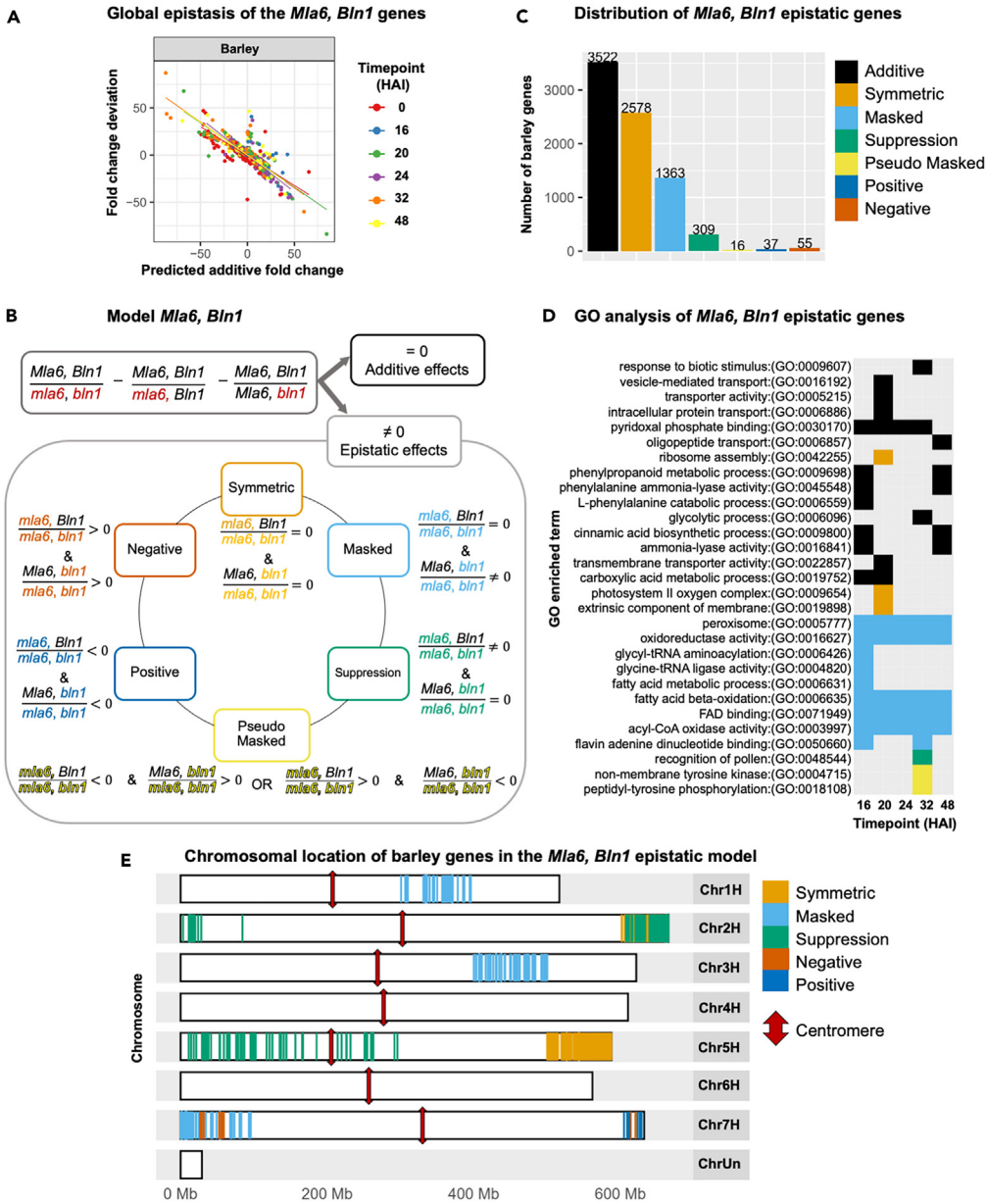

Figure 2. Global and gene-wise epistasis between *Mla6* and *Bln1*

(A) Global epistasis between *Mla6* and *Bln1* in the *Bh*-induced barley transcriptome. The expected additive fold change between the single and double mutant and the observed deviation is plotted and separated by organism and timepoint.

(B) Proposed gene-wise epistasis model between *Mla6* and *Bln1* applied to the *Bh*-induced barley transcriptome. Additive and epistasis effects are separated and then the epistatic effects are classified into six categories.

(C) Distribution of the *Mla6* and *Bln1* epistatic classifications for the *Bh*-induced barley transcriptome.

(D) Gene Ontology (GO) enrichment analysis of the barley epistatic patterns applied to the transcriptome across time.

(E) Enriched chromosomal locations of the barley genes under the *Mla6*, *Bln1* epistatic model. Each barley chromosome is shown, and colored areas correspond to the different genetic patterns that are significantly enriched (adjusted *p*-value<0.005). Morex V3 centromere positions[70] are indicated by double ended red arrows.

obtaining values of −0.78 to −0.62. These values (different than zero) indicate symmetric epistasis between *Mla6* and *Bln1*, and stronger genetic effects of *Mla6* (negative slope values) on barley gene expression.

To explore the transcriptional effects of *Mla6* and *Bln1* at the gene level, we applied an epistasis classification model. As illustrated in Figure 2B, the model includes additive and interaction effects, and those patterns with non-additive effects are further classified into six

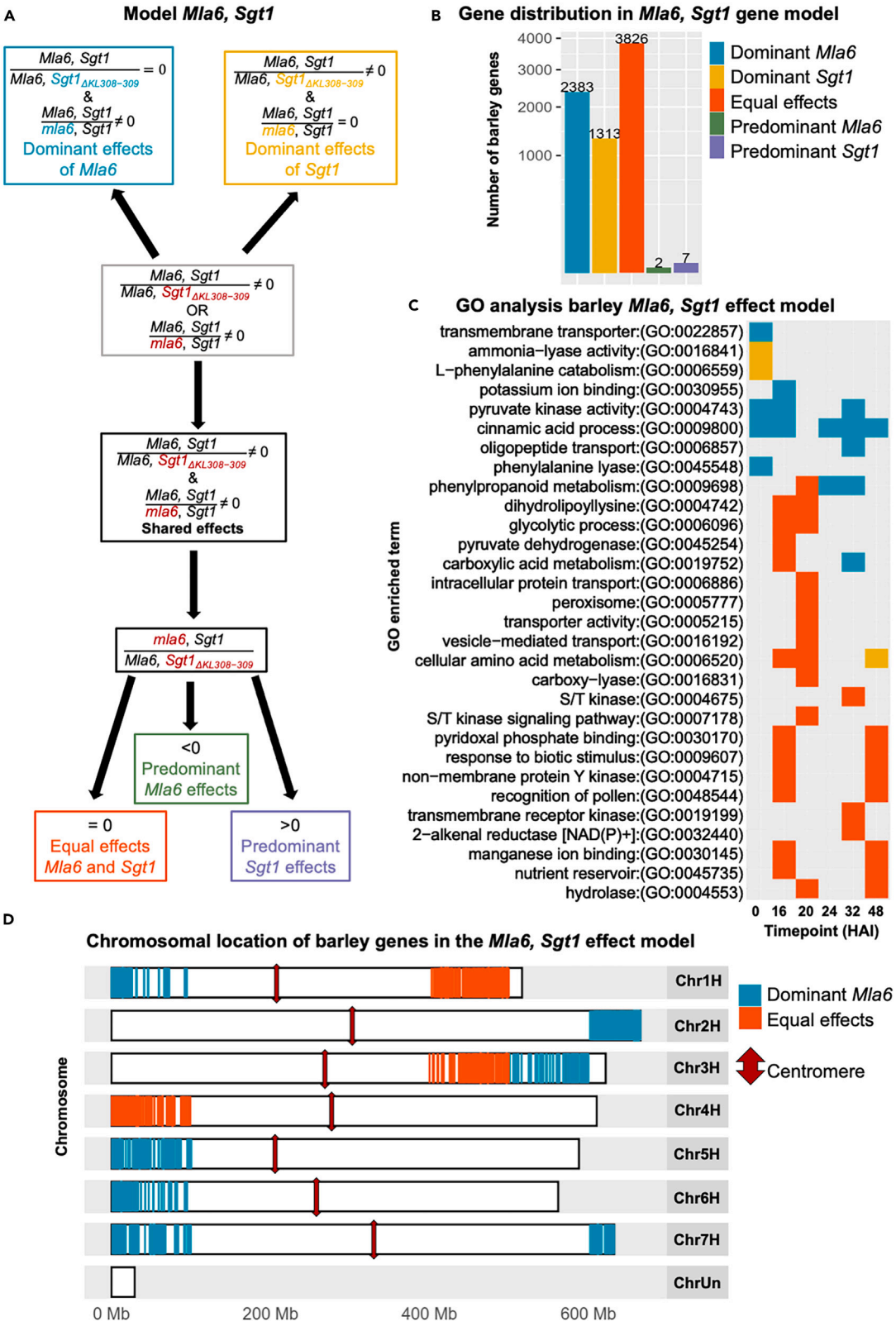
A
Model Mla6, Sgt1
Mla6, Sgt1 / Mla6, Sgt1ΔKL308-309 = 0 & Mla6, Sgt1 / mla6, Sgt1 ≠ 0
Dominant effects of Mla6
Mla6, Sgt1 / Mla6, Sgt1ΔKL308-309 ≠ 0 & Mla6, Sgt1 / mla6, Sgt1 = 0
Dominant effects of Sgt1
Mla6, Sgt1 / Mla6, Sgt1ΔKL308-309 ≠ 0 OR Mla6, Sgt1 / mla6, Sgt1 ≠ 0
Mla6, Sgt1 / Mla6, Sgt1ΔKL308-309 ≠ 0 & Mla6, Sgt1 / mla6, Sgt1 ≠ 0
Shared effects
mla6, Sgt1 / Mla6, Sgt1ΔKL308-309
<0
Predominant Mla6 effects
= 0
Equal effects Mla6 and Sgt1
>0
Predominant Sgt1 effects
B
Gene distribution in Mla6, Sgt1 gene model
Number of barley genes
4000
3000
2000
1000
2383
1313
3826
2
7
Dominant Mla6
Dominant Sgt1
Equal effects
Predominant Mla6
Predominant Sgt1
C
GO analysis barley Mla6, Sgt1 effect model
GO enriched term
transmembrane transporter:(GO:0022857)
ammonia−lyase activity:(GO:0016841)
L−phenylalanine catabolism:(GO:0006559)
potassium ion binding:(GO:0030955)
pyruvate kinase activity:(GO:0004743)
cinnamic acid process:(GO:0009800)
oligopeptide transport:(GO:0006857)
phenylalanine lyase:(GO:0045548)
phenylpropanoid metabolism:(GO:0009698)
dihydrolipoyllysine:(GO:0004742)
glycolytic process:(GO:0006096)
pyruvate dehydrogenase:(GO:0045254)
carboxylic acid metabolism:(GO:0019752)
intracellular protein transport:(GO:0006886)
peroxisome:(GO:0005777)
transporter activity:(GO:0005215)
vesicle−mediated transport:(GO:0016192)
cellular amino acid metabolism:(GO:0006520)
carboxy−lyase:(GO:0016831)
S/T kinase:(GO:0004675)
S/T kinase signaling pathway:(GO:0007178)
pyridoxal phosphate binding:(GO:0030170)
response to biotic stimulus:(GO:0009607)
non−membrane protein Y kinase:(GO:0004715)
recognition of pollen:(GO:0048544)
transmembrane receptor kinase:(GO:0019199)
2−alkenal reductase [NAD(P)+]:(GO:0032440)
manganese ion binding:(GO:0030145)
nutrient reservoir:(GO:0045735)
hydrolase:(GO:0004553)
0 16 20 24 32 48
Timepoint (HAI)
D
Chromosomal location of barley genes in the Mla6, Sgt1 effect model
Chromosome
Chr1H
Chr2H
Chr3H
Chr4H
Chr5H
Chr6H
Chr7H
ChrUn
0 Mb
200 Mb
400 Mb
600 Mb
Dominant Mla6
Equal effects
Centromere

Figure 3. Genetic effects model of *Mla6* and *Sgt1*

(A) Proposed effect model between *Mla6* and *Sgt1* in the *Bh*-induced barley transcriptome. Effects are separated into dominant effects where only one of the mutant genotypes has significant differences; equal effects where both mutants have the same effects and predominant effects where the strength of the differences is higher in one of the mutants.

(B) Distribution and (C) GO enrichment across time of the model classifications for the *Bh*-induced barley transcriptome.

(D) Enriched chromosomal locations of the barley genes under the *Mla6*, *Sgt1* epistatic model. Each barley chromosome is shown, and colored areas correspond to the significantly enriched genetic patterns (adjusted *p*-value<0.005). Morex V3 centromere positions[70] are indicated by double ended red arrows.

categories.[62,71] These include symmetric epistasis, where both single and double mutants have the same effect; masked and suppression epistasis where the expression of the double mutant is equal to one of the single mutants (*mla6*-m18982 and *bln1*-m19089, respectively); pseudo masked epistasis, where the expression of the double mutant is between the two single mutants. Two additional classes were found where the double mutant has a higher (positive epistasis) or lower (negative epistasis) expression than the single mutants.

These classifications were applied to our RNA-Seq dataset, separated by timepoint. To generate a consensus of the epistasis patterns across time, we used the most frequent classification across all timepoints for each gene (excepting 0 HAI), and then summarized the results as shown in Figure 2C (full list in Table S2). We determined that the 0 HAI timepoint introduced error into the consensus because of artificially low read counts, resulting in large differences observed in the PCA analysis with other timepoints (Figure 1B).[72] Subsequently, the ensuing dataset would have a higher false positive rate for mining DEGs. Most of the barley genes had an additive effect between *Mla6* and *Bln1*, which means they did not go through epistasis. Among the epistatic genes, we found that most had a symmetric pattern followed by masking and suppression. These results coincide with what we observed in the genome-wide epistasis analysis presented in Figure 2A. Smaller sets of genes presented pseudo masked, positive, and negative epistasis.

We then performed Gene Ontology (GO) analysis to describe the biological functions of the genes under each epistasis pattern, as shown in Figure 2D. Additive effects of *Mla6* and *Bln1* targeted genes involved in intracellular and membrane transport, MAP and receptor kinase, response to stimulus, chloroplast, and carbohydrate binding. These additive effects were found across the entire time course, with higher frequency at 16 and 48 HAI, which are associated with the *Bh* penetration and formation of haustoria, respectively. Among epistatic patterns, symmetric epistasis was associated with genes at 20 HAI, which are involved in the ribosomal, photosynthetic, and extrinsic components of the membrane. Pseudo-masked and suppression epistasis influenced genes at 32 HAI, which were involved in the phosphorylation and recognition of pollen. Lastly, masked epistasis presented an influence across the time course, and the genes under this pattern were associated with oxidoreductase activity, peroxisome, translation, fatty acid, and acyl CoA metabolism.

Epistasis effects cluster at chromosome hotspots

After finding evidence of genetic interaction between *Mla6* and *Bln1*, we explored possible mechanisms of the regulation of such patterns by looking for an association between the genes under each pattern and their genomic location (see STAR Methods). Taking genome windows of 1 Mb, 10 Mb, 100 Mb, and the complete chromosome we tested for the enrichment of genes classified in each of the categories for each model while correcting for the gene density in each bin. We found significant genomic hotspots associated with each epistasis category as shown in Figure 2E and Table S3, distributed across chromosomes 1H–3H and 5H–7H. Genes under symmetric epistasis were concentrated in chromosomal 100 Mb windows 2H.6 (designating chr 2H, positions 600–700 Mb), and 5H.5 (chr 5H, positions 500–600 Mb). Masked epistasis had effects on genes concentrated in the regions 1H.3 (chr 1H, positions 300–400 Mb), 3H.4 (chr 3H, positions 400–500 Mb) and 7H.0 (chr 7H, positions 0–100 Mb) whereas genes under suppression were associated with regions 2H.0, 2H.6 and a wide range on chromosome 5 from 5H.0 to 5H.2. Lastly, genes under negative epistasis were enriched to regions in chromosome 7 (7H.0 and 7H.6). The distribution of the hotspots was diverse, showing high location specificity with two exceptions: region 2H.6 and 7H.0 that were enriched in two epistatic patterns.

In previous work, we presented a protein-protein interaction (PPI) network associated with MLA (MLAInt.[73]; Cross-referencing with these earlier analyses revealed that about half of the nodes in the MLAInt networks overlap with genes under epistasis in the current report. As shown in Table S3, we observed enrichment in MLAInt of genes under symmetric epistasis at hotpots 2H.6 and 5H.5, as well as genes under masked epistasis at locations 1H.3, 3H.4 and 7H.0. Examples of such genes include kinases (2H.6, 3H.4), a WRKY transcription factor (3H.4) and proteasome-associated genes (2H.6, 5H.5, 7H.0).

Design of a *Mla6, Sgt1* gene effect model

We proposed a second classification model for gene expression associated with *Mla6* and *Sgt1* which did not require a double-mutant dataset. However, it should be noted that the MLA6 protein requires SGT1 to function properly, i.e., express resistance to AVR_{a6} containing *Bh* isolates.[43,44] For this second model (*Mla6, Sgt1*), we could not separate additive from epistatic effects, but we could compare the strength of the contribution of each gene to the wild-type genotype. To accomplish this, we used a classification of five categories by separating the effects of *Mla6* and *Sgt1* into dominant, predominant, and equal effects (Figures 3A and 3B). We defined dominant effects as those where only one of the single mutants is differentially expressed as compared to the wild type. For example, genes under dominant effects of *Mla6* were calculated as those that were not DE between the wild-type and *rar3*-m11526 (= $Sgt1_{\Delta KL308\text{-}309}$), and DE when the wild-type was compared to *mla6*-m18982. Then, we further separated the shared effects (genes that are DE in both single mutants), into predominant and equal effects. Predominant effects have significantly higher expression in one of the single mutants as compared to the other one. We defined genes under predominant effects of *Mla6* as those whose expression was higher in *rar3*-m11526 as compared to *mla6*-m18982, as the first contains a wild-type version of the gene, indicating its stronger effect. Lastly, equal effects of *Mla6* and *Sgt1* have the same expression level in both mutants.

Figure 3B shows the distribution of these classifications for the barley transcriptome and the full list is reported in Table S2. Results indicate that most of the DE genes in the barley transcriptome were under equal gene effects of *Mla6* and *Sgt1*, followed by those under the dominant effects of *Mla6* and *Sgt1*. GO enrichment analysis of the genes associated with each classification showed that the expression of genes under the same effects of *Mla6* and *Sgt1* were involved in diverse biological processes across the time course (Figure 3C). Among them, we found serine/threonine and tyrosine kinase, intracellular and vesicle−mediated transport, peroxisome, pyruvate metabolism, phenylalanine ammonia−lyase, response to biotic stimulus and cinnamic acid biosynthesis. Dominant effects of *Mla6* were associated with the expression of genes involved in transmembrane transporter, potassium ion binding, cinnamic acid process, phenylalanine lyase, and phenylpropanoid metabolism. Dominant effects of *Sgt1* were associated with the expression of genes with functions such as L−phenylalanine catabolism and cellular amino acid metabolism.

When the *Mla6, Sgt1* classification model was analyzed for associations with genomic location, we found the enrichment of genes associated with dominant effects of *Mla6* and equal effects of *Mla6* and *Sgt1* (Table S3). Genes associated with dominant effects of *Mla6* were enriched to several regions across six out of seven barley chromosomes (Figure 3D) including 1H.0, 2H.6, 3H.5, 5H.0, 6H.0, 7H.0 and 7H.6. Genes whose expression was equally affected by *Mla6* and *Sgt1* were enriched to three chromosomal regions: 1H.4, 3H.4 and 4H.0. These results indicate that the hotspots associated with dominant effects of *Mla6* were shared with the epistatic patterns in the *Mla6, Bln1* model while other locations were enriched when genetic effects of *Mla6* and *Sgt1* were analyzed. For example, regions 1H.4, 3H.5, and chromosome 4 were only enriched in genes under this type of classification. These results indicate different pathways of each interaction with *Mla6*. At the protein level, MLA and SGT1 interact physically, therefore the MLAInt network contains the signaling associations to both proteins. Enrichment genes under equal effect of both *Mla6* and *Sgt1* were found enriched in MLAInt, including those located to hotspots 1H.4, 3H.4, and 4H.0. Genes under dominant effects of *Mla6* were also enriched and linked to the hotspots 3H.5 and 7H.0, as shown in Table S3. These findings indicate that there is an overlap between the genetic and protein networks that control *Mla6*-specified resistance.

Nucleotide-binding leucine-rich repeat receptor expression is subject to epistatic effects

We explored the effects of epistasis on transcript accumulation that encodes NLRs, key proteins that determine the outcome of barley-*Bh* interactions. The 468 NLRs annotated for the Morex V3 assembly[28] were filtered under each gene effect model. Of these, 366 were present in our expression dataset and 115 were classified under at least one of the models (103 for the *Mla6, Bln1* epistasis model and 90 for the *Mla6, Sgt1* gene effect model). Figure 4 depicts a heatmap for these 115 NLRs across time and genotypes; Data S1 shows the time-course expression graphs of all the expressed NLRs in the CI 16151 progenitor and derived mutants. Using hierarchical clustering we grouped the NLRs and annotated them using the two gene effect models. First, for the *Mla6, Bln1* model we observed that the most common pattern within the NLR group was additive effects followed by symmetric, suppression, and masked epistasis. Forty-four NLRs under additive effects were scattered across the heatmap with four subgroups of more than two members which presented co-expression. The additive epistasis group included NLR genes with very diverse expression patterns. *Mla6* (r3.1HG0012670) belongs to this group, displaying diminished expression in the *mla6* single and *mla6* + *bln1* double mutant (Figure S2).

Similarly, symmetric epistasis was observed in 30 NLR, with a diverse set of expression patterns. We highlight the examples as r3.5HG0526160, where plants harboring single and double mutants of *mla6* and *bln1* were down-regulated as compared to *rar3* or CI 16151; or r3.5HG0526460 with the opposite pattern. Masked epistasis (16 NLRs) had one co-expressed subgroup including representative genes such as r3.7HG0640630 where *mla6* and *bln1* single mutants had intermediate expression, or where in r3.7HG0634870 only the *bln1* mutant had expression counts above zero. Lastly, we also found NLRs whose expression pattern fit suppression (9 NLRs), positive (1 NLR), and negative (3 NLRs) epistasis. Most genes under suppression epistasis showed no significant transcript accumulation in the *mla6* single mutant, including NLRs such as *Pbr1*[74,75]; by contrast, r3.2HG0216800 was not expressed in all other genotypes, except the *mla6* single mutant. One NLR presented positive epistasis (r3.2HG0095950) which did not show significant transcript accumulation except in the (*mla6*+ *bln1*)-m19028 double mutant. Three NLRs presented negative epistasis (r3.7HG0744510, r3.6HG0629180, r3.7HG0744530), and their expression patterns showed higher expression in the single mutants as compared to the double mutant.

When classifications of the *Mla6 and Sgt1* models were analyzed, we found that the clustering separated the dominant effects of *Mla6* and equal effects, while the dominant effects of *Sgt1* were more scattered. We also noticed that the dominant effects of *Sgt1* coincided with symmetric epistasis in the *Mla6, Bln1* model. Among them, we highlight *Rp1*-like r3.6HG0594450, an NLR whose expression is significantly higher for *rar3*-m11526 (*Mla6, Bln1, Sgt1*$_{\Delta KL308\text{-}309}$) over the rest of the genotypes. Equal effects of *Mla6* and *Sgt1* were associated with expression patterns where the susceptible genotypes had low transcript levels while the resistant genotypes presented peaks across the time course. In contrast, the group of NLRs that were classified under dominant effects of *Mla6* exhibited expression patterns where *rar3*-m11526 had a similar expression to the resistant genotypes while the *mla6*-m18982 mutant was significantly different from them, grouping with the double mutant or separating from all the other genotypes.

Differential immunity to *Pseudomonas syringae* pv. *phaseolicola* expressing AvrPphB associates with suppression epistasis of *HvPbr1*, and masked epistasis influences *bln1*-coupled responses to powdery mildew

Suppression- and masked-epistasis are particularly intriguing in terms of their effects on immunity. In suppression epistasis, gene expression is affected by the *mla6* mutation only in combination with the unlinked wild-type *Bln1* gene. Generally, most barley genes under suppression epistasis are downregulated in the *mla6* mutant, when compared with the *mla6* + *bln1* double mutant (Figure 4) and are primarily clustered at

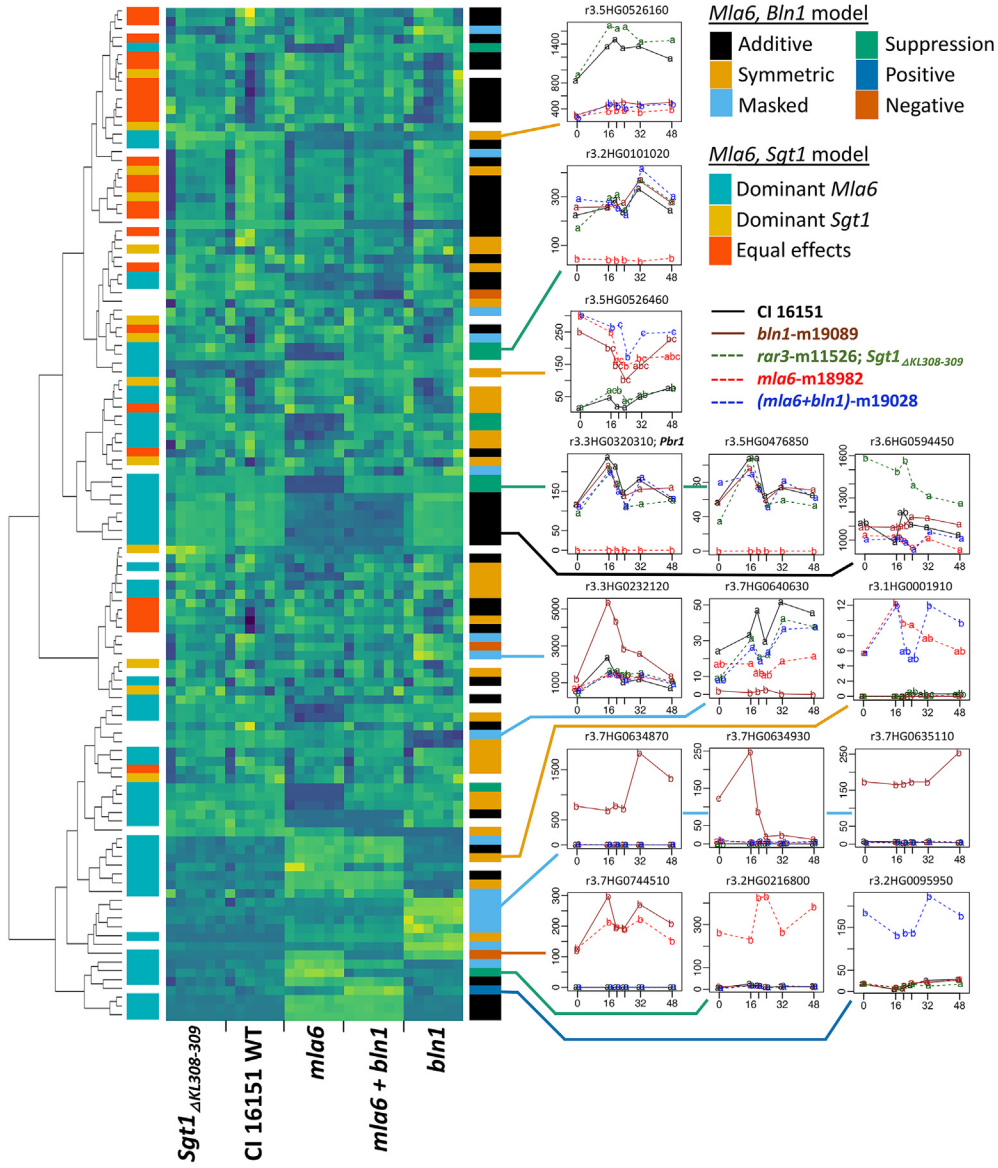

Figure 4. Heatmap of the barley NLRs classified in the *Mla6, Bln1* or *Mla6, Sgt1* gene effect models

Time-course expression of barley NLRs were hierarchically clustered and plotted with a heatmap. Annotation of *Mla6, Bln1*, and *Mla6, Sgt1* models are shown at the right and left of the heatmap, respectively. Lastly, examples from each group were plotted with expression patterns as indicated by legend color. An adjusted *p*-value cutoff of 0.001, as designated by lower case letters a, b, and c, was used to assign significant differences in expression.

the telomeric ends of chromosome 2H, and the top half of chromosome 5H (Figure 2E). This is exemplified by the barley NLR, AvrPphB Response 1 (HvPBR1), which specifies recognition to the effector protease AvrPphB from *P. syringae* pv. *phaseolicola*.[74]

We tested the suppression epistasis effect on immunity by challenging the wild-type progenitor CI 16151 (*Mla6*), the two single mutants *mla6*-m18982 and *bln1*-m19089, as well as the double mutant (*mla6 + bln1*)-m19028, by the infiltration of *P. syringae* expressing AvrPphB. As illustrated in Figure 5B and Figure S4, CI 16151 elicits a weak chlorotic response (LC) when challenged with AvrPphB, as documented previously by Carter and colleagues[74] and encircled by a magenta box. In addition, the loss-of-function *mla6* mutant exhibited no response to AvrPphB (N), which associates with the lack of observed *Pbr1* transcripts in this genotype (Figure 5A). However, the *mla6 + bln1* double mutant displayed an equivalent response (LC) to the CI 16151 wildtype. The *bln1* single mutant also displayed an LC response, which would be expected since this genotype also contains *Mla6*. Taken together, these immune responses to the effector AvrPphB are consistent with suppression epistasis manifested by the genetic interactions of *mla6* and *bln1* on *Pbr1* transcript accumulation.

Then, to test *mla6* and *bln1* influenced epistasis on immunity to powdery mildew, we challenged plants with CC148, a non-*Mla6* recognizing isolate of *Bh*. CC148 is virulent on CI 16151 progenitor plants, and accordingly, allowed us to view *Bh* infection independent of

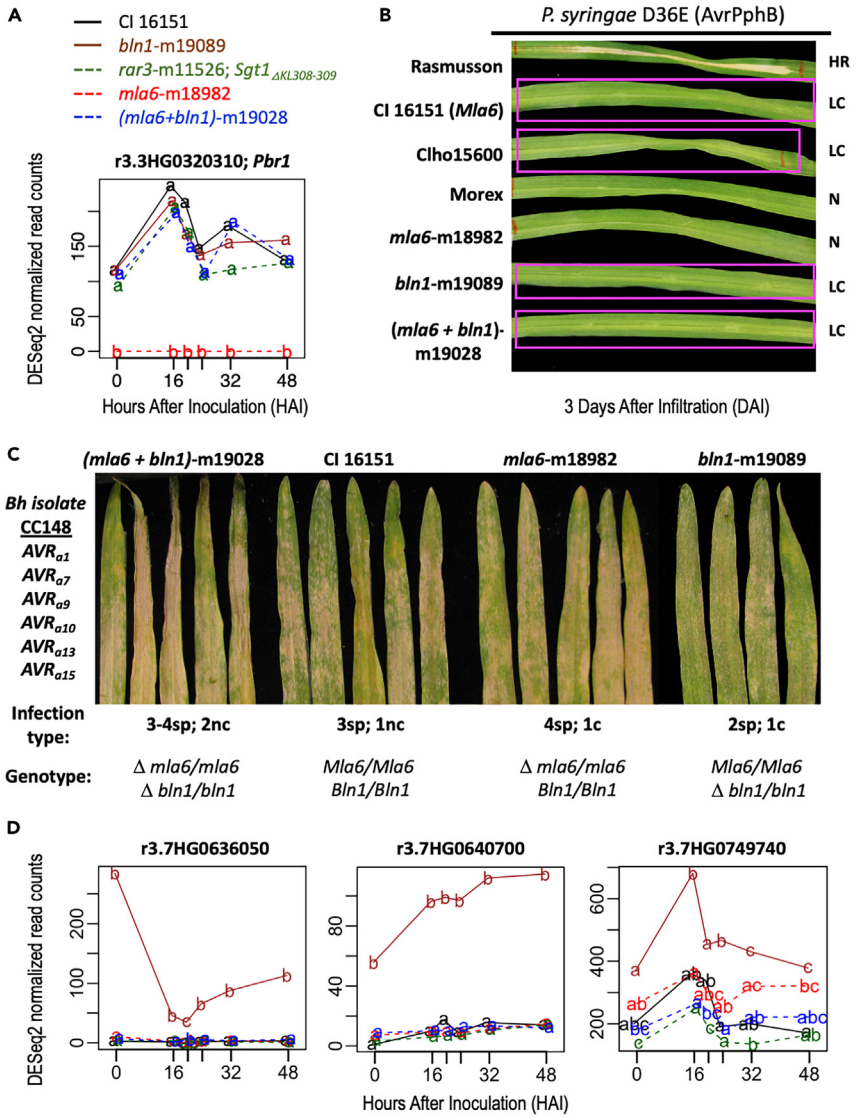

Figure 5. Differential immunity of barley to *P. syringae* pv. *phaseolicola* expressing AvrPphB associates with suppression epistasis of *HvPbr1*

(A) Time-course expression of *HvPbr1* transcripts as determined by the RNA sequencing of CI 16151 and derived mutants (see STAR Methods). Significant differences, as designated by lower case letters a and b, were determined by a *p*-value cutoff of 0.001.

(B) *P. syringae* DC3000 D36E uniquely expressing the effector AvrPphB was syringe-infiltrated into the adaxial surface of the L2 leaf of 10-day-old barley. After 3 days, infiltrated leaves were harvested, photographed under white light, and scored according to Carter and colleagues[74] using a predefined scale: no immune response (N), low chlorosis (LC), chlorosis (C), high chlorosis (HC), or hypersensitive reaction (HR).

(C) *Bh* CC148 inoculation of first leaf seedlings of *mla6* and *bln1* single and double mutants, and progenitor CI 16151. Plants were photographed at 6 days after inoculation (DAI) along with their designated macroscopic phenotype and sporulation score. An infection type of 0 is resistant (no sporulation), 1–2 is considered resistant, but with minor *Bh* colonization (sp), and an infection type of 3–4 is susceptible (abundant sporulation). 1n, few small necrotic flecks (0.5 mm); 1–2n, significant small necrotic flecks (1 mm); 2N, abundant cell death (>2 mm); c, limited chlorosis; C, abundant chlorosis.

(D) Time-course expression of NLR transcripts under masked epistasis as determined by RNA sequencing of CI 16151 and derived mutants. Significant differences, as designated by lower case letters a, b, and c, were determined by a *p*-value cutoff of 0.001. Four additional NLRs under masked epistasis (with significantly higher transcript accumulation in the *bln1* mutant; r3.3HG0232120, r3.7HG0634870, r3.7HG0634930, r3.7HG0635110) are shown in Figure 4.

Mla6-AVR$_{a6}$ recognition normally seen with *Bh* 5874. Consistent with the negative regulatory role of *Bnl1*[65], we observed that the *bln1* single mutant was less susceptible than the CI 16151 control and similar to previous virus induced gene silencing of *Bln1* in compatible interactions.[65,66] Interestingly, the *mla6* + *bln1* double mutant had the most severe reaction with the tips of the plants undergoing partial cell death (Figure 5C). Such differential immune response can be categorized as masked epistasis, as the *bln1* mutant differs from the other mutants and the CI 16151 progenitor.

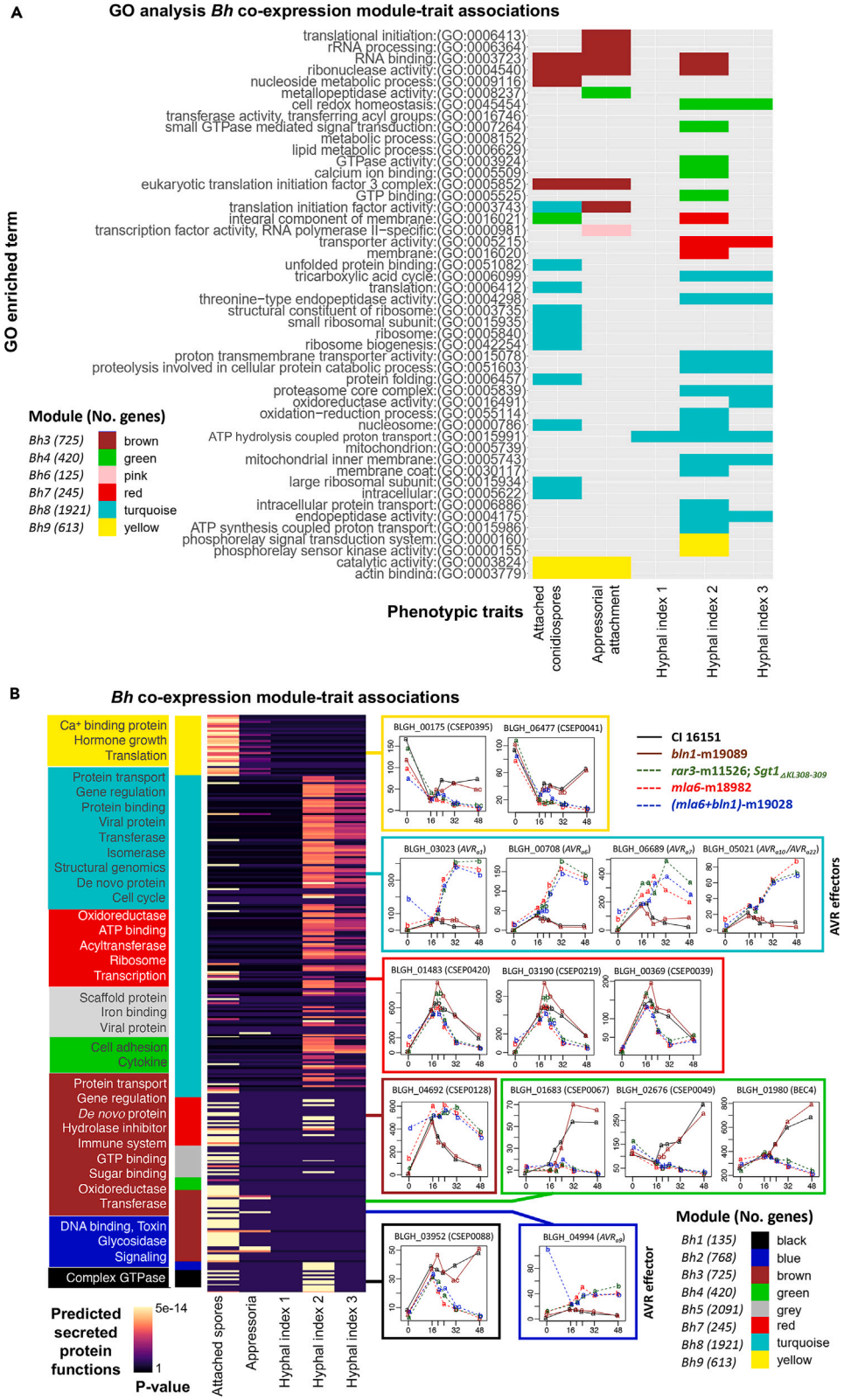
A
GO analysis Bh co-expression module-trait associations
GO enriched term
translational initiation:(GO:0006413)
rRNA processing:(GO:0006364)
RNA binding:(GO:0003723)
ribonuclease activity:(GO:0004540)
nucleoside metabolic process:(GO:0009116)
metallopeptidase activity:(GO:0008237)
cell redox homeostasis:(GO:0045454)
transferase activity, transferring acyl groups:(GO:0016746)
small GTPase mediated signal transduction:(GO:0007264)
metabolic process:(GO:0008152)
lipid metabolic process:(GO:0006629)
GTPase activity:(GO:0003924)
calcium ion binding:(GO:0005509)
eukaryotic translation initiation factor 3 complex:(GO:0005852)
GTP binding:(GO:0005525)
translation initiation factor activity:(GO:0003743)
integral component of membrane:(GO:0016021)
transcription factor activity, RNA polymerase II-specific:(GO:0000981)
transporter activity:(GO:0005215)
membrane:(GO:0016020)
unfolded protein binding:(GO:0051082)
tricarboxylic acid cycle:(GO:0006099)
translation:(GO:0006412)
threonine-type endopeptidase activity:(GO:0004298)
structural constituent of ribosome:(GO:0003735)
small ribosomal subunit:(GO:0015935)
ribosome:(GO:0005840)
ribosome biogenesis:(GO:0042254)
proton transmembrane transporter activity:(GO:0015078)
proteolysis involved in cellular protein catabolic process:(GO:0051603)
protein folding:(GO:0006457)
proteasome core complex:(GO:0005839)
oxidoreductase activity:(GO:0016491)
oxidation-reduction process:(GO:0055114)
nucleosome:(GO:0000786)
ATP hydrolysis coupled proton transport:(GO:0015991)
mitochondrion:(GO:0005739)
mitochondrial inner membrane:(GO:0005743)
membrane coat:(GO:0030117)
large ribosomal subunit:(GO:0015934)
intracellular:(GO:0005622)
intracellular protein transport:(GO:0006886)
endopeptidase activity:(GO:0004175)
ATP synthesis coupled proton transport:(GO:0015986)
phosphorelay signal transduction system:(GO:0000160)
phosphorelay sensor kinase activity:(GO:0000155)
catalytic activity:(GO:0003824)
actin binding:(GO:0003779)
Module (No. genes)
Bh3 (725) brown
Bh4 (420) green
Bh6 (125) pink
Bh7 (245) red
Bh8 (1921) turquoise
Bh9 (613) yellow
Phenotypic traits
Attached conidiospores
Appressorial attachment
Hyphal index 1
Hyphal index 2
Hyphal index 3
B
Bh co-expression module-trait associations
Ca+ binding protein
Hormone growth
Translation
Protein transport
Gene regulation
Protein binding
Viral protein
Transferase
Isomerase
Structural genomics
De novo protein
Cell cycle
Oxidoreductase
ATP binding
Acyltransferase
Ribosome
Transcription
Scaffold protein
Iron binding
Viral protein
Cell adhesion
Cytokine
Protein transport
Gene regulation
De novo protein
Hydrolase inhibitor
Immune system
GTP binding
Sugar binding
Oxidoreductase
Transferase
DNA binding, Toxin
Glycosidase
Signaling
Complex GTPase
Predicted secreted protein functions
5e-14
1
P-value
Attached spores
Appressoria
Hyphal index 1
Hyphal index 2
Hyphal index 3
BLGH_00175 (CSEP0395)
BLGH_06477 (CSEP0041)
CI 16151
bln1-m19089
rar3-m11526; Sgt1 ΔKL308-309
mla6-m18982
(mla6+bln1)-m19028
BLGH_03023 (AVRa1)
BLGH_00708 (AVRa6)
BLGH_06689 (AVRa7)
BLGH_05021 (AVRa10/AVRA22)
AVR effectors
BLGH_01483 (CSEP0420)
BLGH_03190 (CSEP0219)
BLGH_00369 (CSEP0039)
BLGH_04692 (CSEP0128)
BLGH_01683 (CSEP0067)
BLGH_02676 (CSEP0049)
BLGH_01980 (BEC4)
BLGH_03952 (CSEP0088)
BLGH_04994 (AVR09)
AVR effector
Module (No. genes)
Bh1 (135) black
Bh2 (768) blue
Bh3 (725) brown
Bh4 (420) green
Bh5 (2091) grey
Bh7 (245) red
Bh8 (1921) turquoise
Bh9 (613) yellow

Figure 6. The *Bh* co-expression network is associated with fungal developmental stages

(A) GO enrichment analysis of the significant module-trait associations of the *Bh* transcriptome co-expression network. Modules associated with phenotypic traits include developmental stages (spores, appressorium attachment, and hyphal indexes 1–3).

(B) Significantly associated effectors with phenotypic traits, color represents *p*-value in the hypergeometric test. On the left, the functional prediction of the effectors in each module; on the right, are expression patterns of the representative effectors per module. An adjusted *p*-value cutoff of 0.003, as designated by lower case letters a, b, and c, was used to assign significant differences in expression.

We hypothesize that the action of one or more NLRs classified under masked epistasis could explain the observed phenotypic response. For example, in contrast to the *Pbr1* experiment that was performed using *P. syringae* D36E that expressed only AvrPphB, *Bh* CC148 contains a large effector repertoire. Moreover, seven NLRs under masked epistasis displayed significantly higher transcript accumulation in the *bln1* mutant as compared to the rest of the genotypes (Figure 4 r3.3HG0232120, r3.7HG0634870, r3.7HG0634930, r3.7HG0635110; Figure 5D r3.7HG0749740, r3.7HG0636050, r3.7HG0640700). As previously reported for rice - *M. oryzae* interactions,[76] these expression patterns are in agreement with what may be expected for cross-reactivity in an NLR-effector recognition leading to a partial immune response.

Changes in pathogen expression are due to the environment that the fungus perceives, rather than an epistatic effect from the host genes

Considering that the *Bh* genotype is constant in the experiment, changes in its transcriptome would be the result of the interaction, which could be either compatible (susceptible for host, virulent for pathogen) or incompatible (resistant for host, avirulent for pathogen). As we observe in Figure 1, the *Bh*-infection transcriptome is associated with the disease phenotype, which led us to select a co-expression network as the modeling method to explore the pathogen response. This analysis enables the association of the gene expression patterns in clusters and their functional association with phenotypic traits (in this case, infection structures over time). The *Bh* co-expression network was constructed using WGCNA[77] using gene counts for all 90 samples and replicates. We identified nine clusters in the network, designated *Bh*1 (black; 135 genes), *Bh*2 (blue; 768 genes), *Bh*3 (brown; 725 genes), *Bh*4 (green; 420 genes), *Bh*5 (gray; 2091 genes), *Bh*6 (pink; 125 genes), *Bh*7 (red; 245 genes), *Bh*8 (turquoise; 1921 genes), and *Bh*9 (yellow; 613 genes). For functional characterization, we performed GO analysis using Interproscan[78] and completed an enrichment test for each cluster, as shown in Figure S5.

Among the enriched GO terms per cluster, we found RNA binding for *Bh*3 (brown); oxidoreductase and lipid metabolism for *Bh*4 (green); protein kinase and nuclease activity for *Bh*5 (gray); transcription for *Bh*6 (pink), proteolysis and ribosomal for *Bh*8 (turquoise), and catalytic activity for *Bh*9 (yellow). Genes in the co-expression network were then correlated to quantitative differences in fungal development by WGCNA.[77] As documented in Table S4, traits comprised microscopic quantification of fungal structures including attached conidiospores, appressorium attachment, and hyphal indexes 1, 2, and 3; observed at 16, 20, 24, 28, 32, and 48 HAI.[43]

At the infection kinetics level, significant differences were only found when resistant vs. susceptible genotypes were compared,[43] indicating that the *Bh* phenotype follows a similar response as the transcriptome. However, as shown in Table S5, significant associations between the co-expression clusters and the phenotypic traits were identified at the gene level. First, spore and appressorium attachment had multiple associations with several modules, with opposite correlation signs, while the associations with hyphal indexes were more gene specific. *Bh*5 (gray) and *Bh*9 (yellow) clusters were exclusively associated with spore and appressorium attachments, while *Bh*1 (black), *Bh*3 (brown), *Bh*7 (red), and *Bh*8 (turquoise), were associated with other stages.

GO analysis of the genes and clusters associated with each *Bh* stage is shown in Figure 6A. The number of spores across the time course was associated with actin binding and catalytic activity for *Bh*9 (yellow), translation, protein folding, and ribosome for *Bh*8 (turquoise), and RNA binding and translation for *Bh*3 (brown). Appressorium attachments had associations with actin binding for *Bh*9 (yellow), transcription factor activity for *Bh*6 (pink), translation and RNA processing for *Bh*3 (brown), and metallopeptidase activity for *Bh*4 (green). Hyphal index 1 was associated with ATP hydrolysis coupled proton transport for *Bh*8 (turquoise). Hyphal indexes 2 and 3 had common associations with *Bh*8 (turquoise), including endopeptidase and oxidoreductase activity, proteasome, and proton transmembrane transporter activity. In addition, hyphal indexes had associations with transported activity for *Bh7* (red) and redox activity for *Bh*4 (green). Hyphal index 2 was also associated with GTP binding and GTPase activity for the *Bh*4 (green), and ribonuclease activity for *Bh*3 (brown).

Effector proteins secreted by pathogens modulate, inhibit, or accelerate host processes to enable nutrient acquisition and colonization.[79,80] From the *Bh* list containing 893 effectors/secreted proteins, as reported by,[49,50] 864 were expressed in our dataset. We characterized these secreted proteins using predicted functions from[49,50] and performing hypergeometric tests for enrichment in each of the modules. The modules that were enriched with secreted proteins included *Bh*7 (red), *Bh*8 (turquoise) and *Bh*3 (brown). The *Bh*7 (red) module was enriched in predicted effector functions including proteasome, periplasmic binding protein, ribosome, and transcription. In the *Bh*8 (turquoise) module we found enrichment for protein transport, gene regulation, and protein binding, while effectors in the *Bh*3 (brown) module were associated with gene regulation, *de novo* protein, hydrolase inhibitor, and immune system.

When effector expression patterns were analyzed, we found they were associated with disease phenotype, with a separation between resistant vs. susceptible genotypes. We explored the associations between secreted proteins with the phenotypic traits and characterized them functionally for their role during infection. Figure 6B and Table S5 contain the enriched functions and associations with phenotypic traits. Here, we highlight effector expression patterns starting with AVRs, *e.g.*, BLGH_00708 [identified as AVR_{a6} and representing a group of effectors from the *Bh*8 module (turquoise)], which is significantly associated with attached spores, and hyphal index 1, 2, and 3. Its expression is significantly higher in susceptible backgrounds after penetration as compared to resistant hosts. Other AVR effectors that fit this expression pattern include BLGH_03023 (AVR_{a1}; associated with spores, hyphal index 1,2,3), BLGH_05021 (AVR_{a10}/AVR_{a22}; associated with spores, hyphal

index 1,2,3), and BLGH_06689 (AVR_{a7}; associated with spores). BLGH_04994 (AVR_{a9}) was classified in the *Bh2* (blue) cluster with a similar expression pattern but was not associated with any infection kinetics traits.

Among the effectors classified from the *Bh9* (yellow) module we identified BLGH_00175 (CSEP0395) and BLGH_06477 (CSEP0041) as associated with spores and appressorial attachments; these have lower expression after penetration in susceptible as compared to resistant genotypes. Lastly, we found an expression pattern consistent with a peak at penetration followed by a drop in either the resistant or the susceptible background, with significant differences for timepoints after the peak. Examples of this pattern include BLGH_01483 (CSEP0420), BLGH_03190 (CSEP0219), and BLGH_00369 (CSEP0039) from the *Bh7* (red) module and associated with spores and/or hyphal index 2 and 3.

DISCUSSION

Epistasis and nucleotide-binding leucine-rich repeat receptor expression

Quantitative transcriptome data can be used to evaluate a wide variety of biological questions, beyond conventional differential expression analysis. We utilized our barley immune mutant collection, all derived from a single progenitor, to develop a custom analysis to interrogate the interactions between barley and powdery mildew from the perspective of gene effect models and co-expression.

The first (*Mla6*, *Bln1*) gene effect model leveraged single and double mutants of the NLR-type resistance gene *Mla6*[19,81] and the cysteine-rich, Ca2+ influx reducing peptide encoded by *Bln1*.[65–67] *Bln1* negatively regulates barley basal defense independent of *Mla6*-specified effector triggered immunity (ETI).[65] This allowed us to test the genetic interactions between the two individual resistance mechanisms. In this case, we evaluated epistasis with both a global and a gene-wise estimation. The two analyses were consistent, though, the gene-wise model facilitated the identification of specific epistasis patterns per gene and the subsequent functional classification and chromosomal location of each set. We then found that genes influenced by epistatic interactions at the genetic level overlap with previously discovered PPI immunity networks[73] (Table S3).

In an intriguing example of suppression epistasis, gene expression is modified by the loss-of-function *mla6* mutation in combination with the unlinked wild-type *Bln1* gene. Specifically, transcripts encoding the barley NLR, HvPBR1,[74] were significantly downregulated in the *mla6* mutant, but not in the *mla6* + *bln1* double mutant, nor the other genotypes. We postulate that normal *Pbr1* expression is dependent on a functional *Mla*, and this is influenced by *Bln1*. If *mla* is knocked out, *Bln1* has a negative regulatory effect on *Pbr1* expression. However, if *bln1* has also lost function, as observed in the *mla6* + *bln1* double mutant, then *Pbr1* transcript accumulation is restored. This hypothesis is supported by a demonstration of differential PBR1-specified immune response to the effector protease AvrPphB (Figure 5). This also may explain why barley cultivar Morex also does not respond to the infiltration of *P. syringae* expressing AvrPphB, since even though it appears to have a functional *Bln1* gene,[65] its *mla* allele, *RGH1-bcd*, harbors a retrotransposon footprint in the CDS, rendering it non-functional.[19] Nine of the 260 expressed genes with a consensus classification under the "*Mla6*, *Bln1* suppression" epistasis pattern were NLRs, with 8 uniquely downregulated in the *mla6* mutant, and one significantly upregulated (Figure 4; Data S1; Table S2).

Expression of NLRs in the masked category contrasts with suppression, in that a majority are up-regulated in the *bln1* single mutant, as compared to the *mla6* + *bln1* double mutant (Figures 4 and 5D); genes in this group are primarily clustered on chromosomes 1H, 3H, and 7H (Figure 2E). This suggests that in this case, the presence of *Bln1* is necessary to regulate gene expression, but control is released in its absence, except in combination with a mutant *mla6*. Sixteen of the 1,172 expressed transcripts with a consensus classification under the "*Mla6*, *Bln1* masked" epistasis model were NLRs, with seven uniquely up-regulated in the *bln1* mutant, and one significantly down-regulated (Data S1; Table S2). As demonstrated in Figure 5C, the inoculation of the *mla6/bln1* mutant panel with *Bh* CC148 resulted in the *bln1* single mutant being less susceptible than either the *mla6*-or the *mla6* + *bln1* mutants. Unique up-regulation of one or more of the seven NLR candidates in the masked category (Figures 4 and 5D) may provide mechanistic clues to this non-*Mla6* specified partial resistance, as shown before with interactions of rice with *M. oryzae*.[76] Alternatively, the observed phenotype could be due to a susceptibility gene whose masking expression pattern is suppressed in the *bln1* mutant, as compared to the rest of the genotypes. Considering that the *mla6* mutation abolishes ETI, while the *bln1* mutation enhances basal defense,[65,66] we would expect that the masking pattern correlates with genes implicated in immunity. Indeed, genes under masked epistasis were associated with "translation" and "oxidation functions" (Figure 2D).

The second (*Mla6*, *Sgt1*) model uses the mutation of the NLR-type resistance gene *Mla6* (Halterman et al., 2001), but also takes advantage of the *rar3*-m11526 *in-frame* Lys-Leu deletion of *Sgt1*, which selectively disrupts race-specific resistance conditioned by the *Mla6*, *Mla7*, or *Mla12* alleles, but not *Mla1*, *Mla9*, *Mla10*, and *Mla13*.[43,44] This model is designed to illustrate the interaction between *Mla6* and *Sgt1* when data from the double mutant is not available. It is not an epistasis model; however, it classifies gene expression using the wild-type progenitor as a reference, and it quantifies the effects of each single mutant. Previous studies have shown that SGT1 is required for the MLA6-mediated generation of H_2O_2 and the hypersensitive reaction, and whole-plant resistance to AVR_{a6} containing *Bh* isolates.[43,44] We separated these effects into dominant (when changes in expression are only observed in one of the single mutants; predominant (when there is the effect of both genes but one of them is larger than the other; and equal effects (when both genes affect equally the gene expression). By applying these parameters, we could observe that most genes were under equal effects of *Mla6* and *Sgt1* or dominant effects from *Mla6*. This is similar to what was observed from the epistasis model between *Mla6* and *Bln1* (symmetric, followed by masked epistasis). As both *Mla6* and *Sgt1* mutations disrupt resistance to powdery mildew, a large overlap in the number of genes with equal effects from these genes is expected. Physical interaction between the proteins encoded by these genes has been also demonstrated, which is weakened with the mutated $SGT1_{\Delta KL308\text{-}309}$ protein, causing a reduction in MLA6 protein accumulation, and hindering resistance.[44] The GO terms "vesicle-mediated transport," "S/T kinase amino acid" and "carbohydrate metabolism" were associated with the equal effects of *Mla6* and *Sgt1*, which suggests the presence of cellular functions that depend on a common transcriptional pathway, where both genes interact at the physical level.

Genome conformation and gene location

We postulate that chromosomal position is a mechanism for the transcript patterns observed with the different gene effect models. As illustrated in Figures 2E and 3D, most of the gene effect patterns were enriched in telomere-proximal (TP) and gene-rich interior (GRI) chromosome regions. Likewise, *trans*-activation of gene expression has been associated with genome conformation and gene location,[82] where transcription factories nucleate related functions.[83] Indeed, Baker and colleagues[84] used chromatin immunoprecipitation sequencing (ChIP-Seq) to show that markers of chromatin accessibility, such as H3K27me3 and H3K27me1, were associated with the TP and GRI regions. These regions also correspond to high confidence gene annotations of the barley genome.[84] Thus, the described epistatic patterns could influence gene expression through chromatin accessibility.

Besides genome accessibility, we also hypothesize that the differential recruitment of transcriptional machinery through *cis*-regulatory elements may contribute to the association of gene effect patterns with genome location. Activation of transcription factors may be a key mechanism that regulates gene expression under the proposed gene effect models, although more in-depth study is necessary to test this hypothesis. In *Mla*-based disease resistance, protein interactions have been demonstrated between the MLA protein and several transcription factors including WRKY, MYB, basic-helix-loop-helix (bHLH), and homeobox (HB).[73,85–87] These interactions point to a direct mechanism of transcriptome regulation that can be modified by the loss-of-function mutations evaluated in the current report.

Co-expression between *Blumeria hordei* effectors and fungal development

On the pathogen side, we did not find evidence of host-influenced epistasis, but the co-expressed *Bh* infection transcriptome was concordant to disease phenotype. We constructed a *Bh* co-expression network and then associated it with infection kinetics traits via WGCNA[77] (Figure 6; Table S4 and S5). This approach was effective in classifying *Bh* gene expression, as the number of clusters and their separation were well-defined. Early stages were associated with GO terms "metabolism," "translation" and "metallopeptidase activity,"[56,88] whereas later stages were associated with "RNA binding," "GTPase activity," and "proteasome."[11,57,89]

Secreted proteins were distributed among all co-expression clusters, with significant enrichment in *Bh*3 (brown; 725 genes), *Bh7* (red; 246 genes), and *Bh*8 (turquoise; 1921 genes). When associations with infection traits were evaluated, we generally observed that the *Bh*3 (brown; 725 genes), *Bh*4 (green; 420 genes), *Bh*5 (gray; 2091 genes) and *Bh*9 (yellow; 613 genes) clusters were associated with attached conidiospores while *Bh*8 (turquoise; 1921 genes) linked with hyphal indexes 1–3, indicating that the accumulation of transcripts encoding secreted proteins is aligned with the development of *Bh* structures and that these proteins play different roles over time. Finally, previous functional characterization of *Bh* effectors provided another layer of information for our co-expression analysis.[53–55,57,58,90,91] For example, effectors with associations to attached conidiospores and appressoria, including BLGH_00280 (CSEP0079; *Bh8*, turquoise), BLGH_04692 (CSEP0128; *Bh3*, brown), BLGH_01483 (CSEP0420; *Bh7*, red) and BLGH_00600 (CSEP0422; *Bh*8, turquoise) were also found to be involved in early fungal aggressiveness.[56] In addition, BLGH_06477 (CSEP0041; *Bh9*, yellow) was previously found to be highly expressed in the appressorial germ tube.[92]

Our analysis of the *Bh* transcriptome indicates an important role of the effectors associated with hyphal indexes as well, which were mostly classified in the *Bh8* (turquoise) module. This cluster comprises most of the reported AVR candidates and other effectors that have some functional characterization. For example, BLGH_07004 (CSEP0139) and BLGH_06939 (CSEP0182) suppress BAX-induced programmed cell death in *N. benthamiana* and in barley.[91] These two were found to be significantly associated with hyphal indexes 2 and 3, also known as elongating secondary hyphae (ESH), visual indicators of functional haustoria during development.[93] AVR_{a6} was also classified in the *Bh8* cluster. Interestingly, while BLGH_00709 (CSEP0254) has been reported as an AVR_{a6} candidate, *Bh* isolates DH14 also contains two near-identical copies, BLGH_00708 and BLGH_07091.[11] However, in *Bh* 5874, only BLGH_0078 is expressed, and not BLGH_00709 or BLGH_07091. This suggests that different copies of AVR_{a6} can be expressed in an isolate-specific manner.

Limitations of the study

This analysis of epistasis in barley immunity used replicated time-course expression profiling comprising *Bh* appressorium formation, the penetration of epidermal cells, and the development of haustorial feeding structures on a panel of barley immune signaling mutants. In parallel, we quantified *Bh* infection structures, tested immune activation of PBR1 by infiltration with *P. syringae* expressing AvrPphB, and assessed *Bh* response in *bln1* loss-of-function mutants. This generated a large set of candidate genes that are under diverse epistatic control, nonetheless, several questions remain.

1. Do the genes influenced by epistasis, or genes that colocalize to common chromosomal positions, possess shared *cis*-regulatory elements/modules, or common promoters; and does genome accessibility play a role? These would be interesting and noteworthy areas for follow-up studies.
2. Genetic studies have indicated that *Sgt1* is necessary for *Mla7*- and *Mla12*-specified immunity, but not *Mla1* and *Mla13*.[43] What is the global effect of *Sgt1* on transcript accumulation in *Mla7*-and *Mla12*-containing genotypes? To perform these experiments, one would need an extensive backcrossing program or CRISPR-Cas editing to establish a *rar3*-m11526-like mutant ($Sgt1_{\Delta KL308\text{-}309}$) mutant in these backgrounds, since this is the only known non-lethal mutant in *Sgt1*. Previous investigations have provided data to begin to answer these questions, but $Sgt1_{\Delta KL308\text{-}309}$ was unavailable when these experiments were completed.[94,95,96]
3. Could a similar approach be applied to uncover gene interactions in the pathogen? Mutants have been identified by ultraviolet mutagenesis in both *Bh* and *B. graminis* f. sp. *tritici* (*Bgt*), and regulators of AVR genes have been postulated.[97,98] A comprehensive genotype x time infection transcriptome analysis of carefully selected mutants could identify similar patterns of epistasis.[63]

RESOURCE AVAILABILITY

Lead contact

Further information and requests for resources and reagents should be directed to and will be fulfilled by the lead contact, Dr. Roger Wise (roger.wise@usda.gov).

Materials availability

Mutant barley lines generated in this study and *Bh* isolates can be obtained upon request to the lead contact.

Data and code availability

- Infection-time-course RNA-Seq datasets are available at the NCBI-Gene Expression Omnibus (GEO) database. Accession number is listed in the key resources table.
- Supporting code for the analyses can be found in the GitHub repository https://github.com/Wiselab2/Epistasis.
- Any additional information required to reanalyze the data reported in this article is available from the lead contact upon request.

ACKNOWLEDGMENTS

The authors thank Gregory Fuerst for marker assisted selection and verification of the *mla6*, *bln1*, *mla6 + bln1*, and *rar3* mutants, Stefan Kusch for the most up-to-date *Bh* DH14 genome assembly and annotation, Carsten Pedersen for sharing functional annotations for *Bh* CSEPs, Matt Moscou for assistance with the mapping of *Bln1* in the Morex V3 assembly and Martin Mascher for centromere coordinates in Morex V3.[70] Research supported in part by National Science Foundation - Plant Genome Research Program grant 13-39348, USDA-National Institute of Food and Agriculture (NIFA) grant 2020-67013-31184 and USDA-Agricultural Research Service projects 3625-21000-067-00D and 5030-21220-068-000-D to RPW and USDA-ARS project 5020-21220-014-00D to MH. The funders had no role in study design, data collection and analysis, decision to publish, or the preparation of the article. Mention of trade names or commercial products in this publication is solely for the purpose of providing specific information and does not imply recommendation or endorsement by the USDA, NIFA, ARS, or the National Science Foundation. USDA is an equal opportunity provider and employer. This contribution is dedicated to the memory of Albert H. Ellingboe (1931–2024), who inspired us to look beyond expected genetic segregation ratios.

AUTHOR CONTRIBUTIONS

Designed the research: VVZ and RPW. Performed research: VVZ, PS, AC, NJ, and MH. Contributed new analytic/computational tools: VVZ and SS. Analyzed data: VVZ, PS, SS, NJ, MH, and RPW. Wrote the article: VVZ. Edited the article: VVZ and RPW.

DECLARATION OF INTERESTS

The authors declare no competing interests.

STAR★METHODS

Detailed methods are provided in the online version of this paper and include the following:

- KEY RESOURCES TABLE
- EXPERIMENTAL MODEL AND STUDY PARTICIPANT DETAILS
- METHOD DETAILS
  - Transcriptome data collection
  - Transcriptome profiling
  - Differential expression analysis
  - Mutant characterization
  - *In planta* infiltration assay
  - Gene effect models
  - *Bh* infection kinetics
- QUANTIFICATION AND STATISTICAL ANALYSIS
  - Differential expression analysis
  - GO analysis
  - Chromosomal position analysis
  - Comparison between genetic and protein interaction networks
  - Nucleotide-binding leucine-rich repeat (NLR) pattern analysis
  - Co-expression analysis

SUPPLEMENTAL INFORMATION

Supplemental information can be found online at https://doi.org/10.1016/j.isci.2024.111013.

Received: February 26, 2024
Revised: June 27, 2024
Accepted: September 18, 2024
Published: September 21, 2024

REFERENCES

1. Dangl, J.L., Horvath, D.M., and Staskawicz, B.J. (2013). Pivoting the plant immune system from dissection to deployment. Science *341*, 746–751. https://doi.org/10.1126/science.1236011.
2. Oerke, E.C. (2006). Crop losses to pests. J. Agric. Sci. *144*, 31–43. https://doi.org/10.1017/S0021859605005708.
3. Doehlemann, G., Ökmen, B., Zhu, W., and Sharon, A. (2017). Plant pathogenic fungi. Microbiol. Spectr. *5*, 701–726. https://doi.org/10.1128/microbiolspec.funk-0023-2016.
4. Dean, R., Van Kan, J.A.L., Pretorius, Z.A., Hammond-Kosack, K.E., Di Pietro, A., Spanu, P.D., Rudd, J.J., Dickman, M., Kahmann, R., Ellis, J., and Foster, G.D. (2012). The Top 10 fungal pathogens in molecular plant pathology. Mol. Plant Pathol. *13*, 414–430. https://doi.org/10.1111/j.1364-3703.2011.00783.x.
5. Barsoum, M., Sabelleck, B., D. Spanu, P., and Panstruga, R. (2019). Rumble in the effector jungle: candidate effector proteins in interactions of plants with powdery mildew and rust fungi. CRC Crit. Rev. Plant Sci. *38*, 255–279. https://doi.org/10.1080/07352689.2019.1653514.
6. Kemen, E., Gardiner, A., Schultz-Larsen, T., Kemen, A.C., Balmuth, A.L., Robert-Seilaniantz, A., Bailey, K., Holub, E., Studholme, D.J., MacLean, D., and Jones, J.D.G. (2011). Gene gain and loss during evolution of obligate parasitism in the white rust pathogen of *Arabidopsis thaliana*. PLoS Biol. *9*, e1001094. https://doi.org/10.1371/journal.pbio.1001094.
7. Salguero-Linares, J., Serrano, I., Ruiz-Solani, N., Salas-Gómez, M., Phukan, U.J., González, V.M., Bernardo-Faura, M., Valls, M., Rengel, D., and Coll, N.S. (2022). Robust transcriptional indicators of immune cell death revealed by spatiotemporal transcriptome analyses. Mol. Plant *15*, 1059–1075. https://doi.org/10.1016/j.molp.2022.04.010.
8. Jaswal, R., Kiran, K., Rajarammohan, S., Dubey, H., Singh, P.K., Sharma, Y., Deshmukh, R., Sonah, H., Gupta, N., and Sharma, T.R. (2020). Effector biology of biotrophic plant fungal pathogens: current advances and future prospects. Microbiol. Res. *241*, 126567. https://doi.org/10.1016/j.micres.2020.126567.
9. Kwaaitaal, M., Nielsen, M.E., Böhlenius, H., and Thordal-Christensen, H. (2017). The plant membrane surrounding powdery mildew haustoria shares properties with the endoplasmic reticulum membrane. J. Exp. Bot. *68*, 5731–5743. https://doi.org/10.1093/jxb/erx403.
10. Langin, G., Gouguet, P., and Üstün, S. (2020). Microbial effector proteins – a journey through the proteolytic landscape. Trends Microbiol. *28*, 523–535. https://doi.org/10.1016/j.tim.2020.02.010.
11. Bauer, S., Yu, D., Lawson, A.W., Saur, I.M.L., Frantzeskakis, L., Kracher, B., Logemann, E., Chai, J., Maekawa, T., and Schulze-Lefert, P. (2021). The leucine-rich repeats in allelic barley MLA immune receptors define specificity towards sequence-unrelated powdery mildew avirulence effectors with a predicted common RNase-like fold. PLoS Pathog. *17*, e1009223. https://doi.org/10.1371/journal.ppat.1009223.
12. Bourras, S., Praz, C.R., Spanu, P.D., and Keller, B. (2018). Cereal powdery mildew effectors: a complex toolbox for an obligate pathogen. Curr. Opin. Microbiol. *46*, 26–33. https://doi.org/10.1016/j.mib.2018.01.018.
13. Lu, X., Kracher, B., Saur, I.M.L., Bauer, S., Ellwood, S.R., Wise, R., Yaeno, T., Maekawa, T., and Schulze-Lefert, P. (2016). Allelic barley MLA immune receptors recognize sequence-unrelated avirulence effectors of the powdery mildew pathogen. Proc. Natl. Acad. Sci. USA *113*, E6486–E6495. https://doi.org/10.1073/pnas.1612947113.
14. Menardo, F., Praz, C.R., Wicker, T., and Keller, B. (2017). Rapid turnover of effectors in grass powdery mildew (*Blumeria graminis*). BMC Evol. Biol. *17*, 1–14. https://doi.org/10.1186/s12862-017-1064-2.
15. Saur, I.M., Bauer, S., Kracher, B., Lu, X., Franzeskakis, L., Müller, M.C., Sabelleck, B., Kümmel, F., Panstruga, R., Maekawa, T., and Schulze-Lefert, P. (2019). Multiple pairs of allelic MLA immune receptor-powdery mildew AVR_A effectors argue for a direct recognition mechanism. Elife *8*, e44471. https://doi.org/10.7554/eLife.44471.
16. Crean, E.E., Bilstein-Schloemer, M., Maekawa, T., Schulze-Lefert, P., and Saur, I.M.L. (2023). A dominant-negative avirulence effector of the barley powdery mildew fungus provides mechanistic insight into barley MLA immune receptor activation. J. Exp. Bot. *74*, 5854–5869. https://doi.org/10.1093/jxb/erad285.
17. Cao, Y., Kümmel, F., Logemann, E., Gebauer, J.M., Lawson, A.W., Yu, D., Uthoff, M., Keller, B., Jirschitzka, J., Baumann, U., et al. (2023). Structural polymorphisms within a common powdery mildew effector scaffold as a driver of coevolution with cereal immune receptors. Proc. Natl. Acad. Sci. USA *120*, e2307604120. https://doi.org/10.1073/pnas.2307604120.
18. Ngou, B.P.M., Jones, J.D.G., and Ding, P. (2022). Plant immune networks. Trends Plant Sci. *27*, 255–273. https://doi.org/10.1016/j.tplants.2021.08.012.
19. Wei, F., Wing, R.A., and Wise, R.P. (2002). Genome dynamics and evolution of the *Mla* (powdery mildew) resistance locus in barley. Plant Cell *14*, 1903–1917. https://doi.org/10.1105/tpc.002238.
20. Halterman, D.A., Wei, F., and Wise, R.P. (2003). Powdery mildew-induced *Mla* mRNAs are alternatively spliced and contain multiple upstream open reading frames. Plant Physiol. *131*, 558–567. https://doi.org/10.1104/pp.014407.
21. Shen, Q.-H., Zhou, F., Bieri, S., Haizel, T., Shirasu, K., and Schulze-Lefert, P. (2003). Recognition specificity and RAR1/SGT1 dependence in barley *Mla* disease resistance genes to the powdery mildew fungus. Plant Cell *15*, 732–744. https://doi.org/10.1105/tpc.009258.
22. Bieri, S., Mauch, S., Shen, Q.H., Peart, J., Devoto, A., Casais, C., Ceron, F., Schulze, S., Steinbiß, H.H., Shirasu, K., et al. (2004). RAR1 positively controls steady state levels of barley MLA resistance proteins and enables sufficient MLA6 accumulation for effective resistance. Plant Cell *16*, 3480–3495. https://doi.org/10.1105/tpc.104.026682.
23. Halterman, D.A., and Wise, R.P. (2004). A single-amino acid substitution in the sixth leucine-rich repeat of barley MLA6 and MLA13 alleviates dependence on RAR1 for disease resistance signaling. Plant J. *38*, 215–226. https://doi.org/10.1111/j.1365-313X.2004.02032.x.
24. Seeholzer, S., Tsuchimatsu, T., Jordan, T., Bieri, S., Pajonk, S., Yang, W., Jahoor, A., Shimizu, K.K., Keller, B., and Schulze-Lefert, P. (2010). Diversity at the *Mla* powdery mildew resistance locus from cultivated barley reveals sites of positive selection. Mol. Plant Microbe Interact. *23*, 497–509. https://doi.org/10.1094/MPMI-23-4-0497.
25. Stein, J.C., Yu, Y., Copetti, D., Zwickl, D.J., Zhang, L., Zhang, C., Chougule, K., Gao, D., Iwata, A., Goicoechea, J.L., et al. (2018). Genomes of 13 domesticated and wild rice relatives highlight genetic conservation, turnover and innovation across the genus *Oryza*. Nat. Genet. *50*, 285–296. https://doi.org/10.1038/s41588-018-0040-0.
26. Sánchez-Martín, J., and Keller, B. (2021). NLR immune receptors and diverse types of non-NLR proteins control race-specific resistance in *Triticeae*. Curr. Opin. Plant Biol. *62*, 102053. https://doi.org/10.1016/j.pbi.2021.102053.
27. Walkowiak, S., Gao, L., Monat, C., Haberer, G., Kassa, M.T., Brinton, J., Ramirez-Gonzalez, R.H., Kolodziej, M.C., Delorean, E., Thambugala, D., et al. (2020). Multiple wheat genomes reveal global variation in modern breeding. Nature *588*, 277–283. https://doi.org/10.1038/s41586-020-2961-x.
28. Li, Q., Jiang, X.M., and Shao, Z.Q. (2021). Genome-wide analysis of NLR disease resistance genes in an updated reference genome of barley. Front. Genet. *12*, 694682. https://doi.org/10.3389/fgene.2021.694682.
29. Wróblewski, T., Spiridon, L., Martin, E.C., Petrescu, A.J., Cavanaugh, K., Truco, M.J., Xu, H., Gozdowski, D., Pawłowski, K., Michelmore, R.W., and Takken, F.L.W. (2018). Genome-wide functional analyses of plant coiled–coil NLR-type pathogen receptors reveal essential roles of their N-terminal domain in oligomerization, networking, and immunity. PLoS Biol. *16*, e2005821. https://doi.org/10.1371/journal.pbio.2005821.
30. Mondragón-Palomino, M., Stam, R., John-Arputharaj, A., and Dresselhaus, T. (2017). Diversification of defensins and NLRs in *Arabidopsis* species by different evolutionary mechanisms. BMC Evol. Biol. *17*, 1–23. https://doi.org/10.1186/s12862-017-1099-4.
31. Michelmore, R.W., and Meyers, B.C. (1998). Clusters of resistance genes in plants evolve by divergent selection and a birth-and-death process. Genome Res. *8*, 1113–1130. https://doi.org/10.1101/gr.8.11.1113.
32. van Wersch, S., and Li, X. (2019). Stronger When Together: Clustering of Plant NLR Disease resistance Genes. Trends Plant Sci. *24*, 688–699. https://doi.org/10.1016/j.tplants.2019.05.005.
33. Borrelli, G.M., Mazzucotelli, E., Marone, D., Crosatti, C., Michelotti, V., Valè, G., and Mastrangelo, A.M. (2018). Regulation and evolution of NLR genes: a close interconnection for plant immunity. Int. J. Mol. Sci. *19*, 1662. https://doi.org/10.3390/ijms19061662.
34. Jordan, T., Seeholzer, S., Schwizer, S., Töller, A., Somssich, I.E., and Keller, B. (2011). The wheat *Mla* homologue *TmMla1* exhibits an evolutionarily conserved function against powdery mildew in both wheat and barley.

Plant J. *65*, 610–621. https://doi.org/10.1111/j.1365-313X.2010.04445.x.

35. Maekawa, T., Kracher, B., Vernaldi, S., Ver Loren van Themaat, E., and Schulze-Lefert, P. (2012). Conservation of NLR-triggered immunity across plant lineages. Proc. Natl. Acad. Sci. USA *109*, 20119–20123. https://doi.org/10.1073/pnas.1218059109.
36. Periyannan, S., Moore, J., Ayliffe, M., Bansal, U., Wang, X., Huang, L., Deal, K., Luo, M., Kong, X., Bariana, H., et al. (2013). The gene *Sr33*, an ortholog of barley *Mla* genes, encodes resistance to wheat stem rust race Ug99. Science *341*, 786–788.
37. Mago, R., Zhang, P., Vautrin, S., Šimková, H., Bansal, U., Luo, M.-C., Rouse, M., Karaoglu, H., Periyannan, S., Kolmer, J., et al. (2015). The wheat *Sr50* gene reveals rich diversity at a cereal disease resistance locus. Nat. Plants *1*, 15186. https://doi.org/10.1038/nplants.2015.186.
38. Cesari, S., Moore, J., Chen, C., Webb, D., Periyannan, S., Mago, R., Bernoux, M., Lagudah, E.S., and Dodds, P.N. (2016). Cytosolic activation of cell death and stem rust resistance by cereal MLA-family CC-NLR proteins. Proc. Natl. Acad. Sci. USA *113*, 10204–10209. https://doi.org/10.1073/pnas.1605483113.
39. Bettgenhaeuser, J., Herna, I., Green, P., Taylor, J., Smoker, M., Ferguson, J.N., Emmrich, P., Hubbard, A., Bayles, R., Waugh, R., et al. (2021). The barley immune receptor *Mla* recognizes multiple pathogens and contributes to host range. Nat. Commun. *12*, 6915. https://doi.org/10.1038/s41467-021-27288-3.
40. Brabham, H.J., Gómez De La Cruz, D., Were, V., Shimizu, M., Saitoh, H., Hernández-Pinzón, I., Green, P., Lorang, J., Fujisaki, K., Sato, K., et al. (2023). Barley MLA3 recognizes the host-specificity effector Pwl2 from *Magnaporthe oryzae*. Plant Cell *36*, 447–470. https://doi.org/10.1093/plcell/koad266.
41. Leng, Y., Kümmel, F., Zhao, M., Molnár, I., Doležel, J., Logemann, E., Köchner, P., Xi, P., Yang, S., Moscou, M.J., et al. (2023). A barley MLA receptor is targeted by a non-ribosomal peptide effector of the necrotrophic spot blotch fungus for disease susceptibility. Preprint at bioRxiv *2023*, 571418. https://doi.org/10.1101/2023.12.13.571418.
42. Shirasu, K. (2009). The HSP90-SGT1 Chaperone Complex for NLR Immune Sensors. Annu. Rev. Plant Biol. *60*, 139–164. https://doi.org/10.1146/annurev.arplant.59.032607.092906.
43. Chapman, A.V.E., Hunt, M., Surana, P., Velásquez-Zapata, V., Xu, W., Fuerst, G., and Wise, R.P. (2021). Disruption of barley immunity to powdery mildew by an in-frame Lys-Leu deletion in the essential protein SGT1. Genetics *217*, iyaa026. https://doi.org/10.1093/genetics/iyaa026.
44. Chapman, A.V.E., Elmore, J.M., McReynolds, M., Walley, J.W., and Wise, R.P. (2022). SGT1-specific domain mutations impair interactions with the barley MLA6 immune receptor in association with loss of NLR protein. Mol. Plant Microbe Interact. *35*, 274–289. https://doi.org/10.1094/MPMI-08-21-0217-R.
45. Cesari, S., Bernoux, M., Moncuquet, P., Kroj, T., and Dodds, P.N. (2014). A novel conserved mechanism for plant NLR protein pairs: the "integrated decoy" hypothesis. Front. Plant Sci. *5*, 606. https://doi.org/10.3389/fpls.2014.00606.
46. Bentham, A.R., de la Concepcion, J.C., Mukhi, N., Zdrzałek, R., Draeger, M., Gorenkin, D., Hughes, R.K., and Banfield, M.J. (2020). A molecular roadmap to the plant immune system. J. Biol. Chem. *295*, 14916–14935. https://doi.org/10.1074/jbc.REV120.010852.
47. Sun, Y., Zhu, Y.X., Balint-Kurti, P.J., and Wang, G.F. (2020). Fine-tuning immunity: Players and regulators for plant NLRs. Trends Plant Sci. *25*, 695–713. https://doi.org/10.1016/j.tplants.2020.02.008.
48. van Wersch, S., Tian, L., Hoy, R., and Li, X. (2020). Plant NLRs: The whistleblowers of plant immunity. Plant Commun. *1*, 100016. https://doi.org/10.1016/j.xplc.2019.100016.
49. Pedersen, C., van Themaat, E.V.L., McGuffin, L.J., Abbott, J.C., Burgis, T.A., Barton, G., Bindschedler, L.V., Lu, X., Maekawa, T., Weßling, R., et al. (2012). Structure and evolution of barley powdery mildew effector candidates. BMC Genom. *13*, 694. https://doi.org/10.1186/1471-2164-13-694.
50. Frantzeskakis, L., Kracher, B., Kusch, S., Yoshikawa-Maekawa, M., Bauer, S., Pedersen, C., Spanu, P.D., Maekawa, T., Schulze-Lefert, P., and Panstruga, R. (2018). Signatures of host specialization and a recent transposable element burst in the dynamic one-speed genome of the fungal barley powdery mildew pathogen. BMC Genom. *19*, 381. https://doi.org/10.1186/s12864-018-4750-6.
51. Spanu, P.D., Abbott, J.C., Amselem, J., Burgis, T.A., Soanes, D.M., Stüber, K., Ver Loren van Themaat, E., Brown, J.K.M., Butcher, S.A., Gurr, S.J., et al. (2010). Genome expansion and gene loss in powdery mildew fungi reveal tradeoffs in extreme parasitism. Science *330*, 1543–1546. https://doi.org/10.1126/science.1194573.
52. Kusch, S., Ahmadinejad, N., Panstruga, R., and Kuhn, H. (2014). *In silico* analysis of the core signaling proteome from the barley powdery mildew pathogen (*Blumeria graminis* f.sp. *hordei*). BMC Genom. *15*, 843. https://doi.org/10.1186/1471-2164-15-843.
53. Zhang, W.J., Pedersen, C., Kwaaitaal, M., Gregersen, P.L., Mørch, S.M., Hanisch, S., Kristensen, A., Fuglsang, A.T., Collinge, D.B., and Thordal-Christensen, H. (2012). Interaction of barley powdery mildew effector candidate CSEP0055 with the defence protein PR17c. Mol. Plant Pathol. *13*, 1110–1119. https://doi.org/10.1111/j.1364-3703.2012.00820.x.
54. Pliego, C., Nowara, D., Bonciani, G., Gheorghe, D.M., Xu, R., Surana, P., Whigham, E., Nettleton, D., Bogdanove, A.J., Wise, R.P., et al. (2013). Host-induced gene silencing in barley powdery mildew reveals a class of ribonuclease-like effectors. Mol. Plant Microbe Interact. *26*, 633–642. https://doi.org/10.1094/MPMI-01-13-0005-R.
55. Ahmed, A.A., Pedersen, C., Schultz-Larsen, T., Kwaaitaal, M., Jørgensen, H.J.L., and Thordal-Christensen, H. (2015). The barley powdery mildew candidate secreted effector protein CSEP0105 inhibits the chaperone activity of a small heat shock protein. Plant Physiol. *168*, 321–333. https://doi.org/10.1104/pp.15.00278.
56. Aguilar, G.B., Pedersen, C., and Thordal-Christensen, H. (2016). Identification of eight effector candidate genes involved in early aggressiveness of the barley powdery mildew fungus. Plant Pathol. *65*, 953–958. https://doi.org/10.1111/ppa.12476.
57. Pennington, H.G., Jones, R., Kwon, S., Bonciani, G., Thieron, H., Chandler, T., Luong, P., Morgan, S.N., Przydacz, M., Bozkurt, T., et al. (2019). The fungal ribonuclease-like effector protein CSEP0064/BEC1054 represses plant immunity and interferes with degradation of host ribosomal RNA. PLoS Pathog. *15*, e1007620. https://doi.org/10.1371/journal.ppat.1007620.
58. Yuan, H., Jin, C., Pei, H., Zhao, L., Li, X., Li, J., Huang, W., Fan, R., Liu, W., and Shen, Q.H. (2021). The powdery mildew effector CSEP0027 interacts with barley catalase to regulate host immunity. Front. Plant Sci. *12*, 733237. https://doi.org/10.3389/fpls.2021.733237.
59. Li, Z., Velásquez-Zapata, V., Elmore, J.M., Li, X., Xie, W., Deb, S., Tian, X., Banerjee, S., Jørgensen, H.J.L., Pedersen, C., et al. (2024). Powdery mildew effectors AVR_{A1} and BEC1016 target the ER J-domain protein *Hv*ERdj3B required for immunity in barley. Mol. Plant Pathol. *25*, e13463. https://doi.org/10.1111/mpp.13463.
60. Velásquez-Zapata, V., Elmore, J.M., and Wise, R.P. (2023). Bioinformatic analysis of yeast two-hybrid next-generation interaction screen data. In Protein-Protein Interactions: Methods and Protocols, S. Mukhtar, ed. (Springer US), pp. 223–239. https://doi.org/10.1007/978-1-0716-3327-4_20.
61. Mani, R., St. Onge, R.P., Hartman, J.L., 4th, Giaever, G., and Roth, F.P. (2008). Defining genetic interaction. Proc. Natl. Acad. Sci. USA *105*, 3461–3466. https://doi.org/10.1073/pnas.0712255105.
62. Dixon, S.J., Costanzo, M., Baryshnikova, A., Andrews, B., and Boone, C. (2009). Systematic mapping of genetic interaction networks. Annu. Rev. Genet. *43*, 601–625. https://doi.org/10.1146/annurev.genet.39.073003.114751.
63. Angeles-Albores, D., Puckett Robinson, C., Williams, B.A., Wold, B.J., and Sternberg, P.W. (2018). Reconstructing a metazoan genetic pathway with transcriptome-wide epistasis measurements. Proc. Natl. Acad. Sci. USA *115*, E2930–E2939. https://doi.org/10.1073/pnas.1712387115.
64. Blanc, J., Kremling, K.A.G., Buckler, E., and Josephs, E.B. (2021). Local adaptation contributes to gene expression divergence in maize. G3 (Bethesda). *11*, jkab004. https://doi.org/10.1093/g3journal/jkab004.
65. Meng, Y., Moscou, M.J., and Wise, R.P. (2009). *Blufensin1* negatively impacts basal defense in response to barley powdery mildew. Plant Physiol. *149*, 271–285. https://doi.org/10.1104/pp.108.129031.
66. Xu, W., Meng, Y., Surana, P., Fuerst, G., Nettleton, D., and Wise, R.P. (2015). The knottin-like *Blufensin* family regulates genes involved in nuclear import and the secretory pathway in barley-powdery mildew interactions. Front. Plant Sci. *6*, 409. https://doi.org/10.3389/fpls.2015.00409.
67. Guo, S., Zhang, Y., Li, M., Zeng, P., Zhang, Q., Li, X., Xu, Q., Li, T., Wang, X., Kang, Z., and Zhang, X. (2022). TaBln1, a member of the *Blufensin* family, negatively regulates wheat resistance to stripe rust by reducing Ca2 + influx. Plant Physiol. *189*, 1380–1396. https://doi.org/10.1093/plphys/kiac112.

68. Nirmala, J., Dahl, S., Steffenson, B.J., Kannangara, C.G., Von Wettstein, D., Chen, X., and Kleinhofs, A. (2007). Proteolysis of the barley receptor-like protein kinase RPG1 by a proteasome pathway is correlated with *Rpg1*-mediated stem rust resistance. Proc. Natl. Acad. Sci. USA *104*, 10276–10281. https://doi.org/10.1073/pnas.0703758104.
69. Nirmala, J., Drader, T., Lawrence, P.K., Yin, C., Hulbert, S., Steber, C.M., Steffenson, B.J., Szabo, L.J., Von Wettstein, D., and Kleinhofs, A. (2011). Concerted action of two avirulent spore effectors activates *Reaction to Puccinia graminis 1* (*Rpg1*)-mediated cereal stem rust resistance. Proc. Natl. Acad. Sci. USA *108*, 14676–14681. https://doi.org/10.1073/pnas.1111771108.
70. Navrátilová, P., Toegelová, H., Tulpová, Z., Kuo, Y.-T., Stein, N., Doležel, J., Houben, A., Šimková, H., and Mascher, M. (2022). Prospects of telomere-to-telomere assembly in barley: Analysis of sequence gaps in the MorexV3 reference genome. Plant Biotechnol. J. *20*, 1373–1386. https://doi.org/10.1111/pbi.13816.
71. Cordell, H.J. (2002). Epistasis: What it means, what it doesn't mean, and statistical methods to detect it in humans. Hum. Mol. Genet. *11*, 2463–2468. https://doi.org/10.1093/hmg/11.20.2463.
72. Gihawi, A., Ge, Y., Lu, J., Puiu, D., Xu, A., Cooper, C.S., Brewer, D.S., Pertea, M., and Salzberg, S.L. (2023). Major data analysis errors invalidate cancer microbiome findings. Preprint at bioRxiv *2023*, 2023.07.28.550993. https://doi.org/10.1101/2023.07.28.550993.
73. Velásquez-Zapata, V., Elmore, J.M., Fuerst, G., and Wise, R.P. (2022). An interolog-based barley interactome as an integration framework for immune signaling. Genetics *221*, iyac056. https://doi.org/10.1093/genetics/iyac056.
74. Carter, M.E., Helm, M., Chapman, A.V.E., Wan, E., Restrepo Sierra, A.M., Innes, R.W., Bogdanove, A.J., and Wise, R.P. (2019). Convergent evolution of effector protease recognition by *Arabidopsis* and barley. Mol. Plant Microbe Interact. *32*, 550–565. https://doi.org/10.1094/MPMI-07-18-0202-FI.
75. Jaiswal, N., Myers, A., Weese, T.L., Carter, M.E., Scofield, S.R., and Helm, M. (2023). Analysis of cell death induction by the barley NLR immune receptor PBR1. PhytoFront. *15*, 524147. https://doi.org/10.1101/2023.01.15.524147.
76. Varden, F.A., Saitoh, H., Yoshino, K., Franceschetti, M., Kamoun, S., Terauchi, R., and Banfield, M.J. (2019). Cross-reactivity of a rice NLR immune receptor to distinct effectors from the rice blast pathogen *Magnaporthe oryzae* provides partial disease resistance. J. Biol. Chem. *294*, 13006–13016. https://doi.org/10.1074/jbc.RA119.007730.
77. Langfelder, P., and Horvath, S. (2008). WGCNA: An R package for weighted correlation network analysis. BMC Bioinf. *9*, 559. https://doi.org/10.1186/1471-2105-9-559.
78. Jones, P., Binns, D., Chang, H.Y., Fraser, M., Li, W., McAnulla, C., McWilliam, H., Maslen, J., Mitchell, A., Nuka, G., et al. (2014). InterProScan 5: Genome-scale protein function classification. Bioinformatics *30*, 1236–1240. https://doi.org/10.1093/bioinformatics/btu031.
79. Lo-Presti, L., Lanver, D., Schweizer, G., Tanaka, S., Liang, L., Tollot, M., Zuccaro, A., Reissmann, S., and Kahmann, R. (2015). Fungal effectors and plant susceptibility. Annu. Rev. Plant Biol. *66*, 513–545. https://doi.org/10.1146/annurev-arplant-043014-114623.
80. Toruño, T.Y., Stergiopoulos, I., and Coaker, G. (2016). Plant-pathogen effectors: cellular probes interfering with plant defenses in spatial and temporal manners. Annu. Rev. Phytopathol. *54*, 419–441. https://doi.org/10.1146/annurev-phyto-080615-100204.
81. Halterman, D., Zhou, F., Wei, F., Wise, R.P., and Schulze-Lefert, P. (2001). The MLA6 coiled-coil, NBS-LRR protein confers *AvrMla6*-dependent resistance specificity to *Blumeria graminis* f. sp. *hordei* in barley and wheat. Plant J. *25*, 335–348. https://doi.org/10.1046/j.1365-313X.2001.00982.x.
82. Cook, P.R., and Marenduzzo, D. (2018). Transcription-driven genome organization: A model for chromosome structure and the regulation of gene expression tested through simulations. Nucleic Acids Res. *46*, 9895–9906. https://doi.org/10.1093/nar/gky763.
83. Papantonis, A., and Cook, P.R. (2013). Transcription factories: Genome organization and gene regulation. Chem. Rev. *113*, 8683–8705. https://doi.org/10.1021/cr300513p.
84. Baker, K., Dhillon, T., Colas, I., Cook, N., Milne, I., Milne, L., Bayer, M., and Flavell, A.J. (2015). Chromatin state analysis of the barley epigenome reveals a higher-order structure defined by H3K27me1 and H3K27me3 abundance. Plant J. *84*, 111–124. https://doi.org/10.1111/tpj.12963.
85. Chang, C., Yu, D., Jiao, J., Jing, S., Schulze-Lefert, P., and Shen, Q.-H. (2013). Barley MLA immune receptors directly interfere with antagonistically acting transcription factors to initiate disease resistance signaling. Plant Cell *25*, 1158–1173. https://doi.org/10.1105/tpc.113.109942.
86. Shen, Q.H., Saijo, Y., Mauch, S., Biskup, C., Bieri, S., Keller, B., Seki, H., Ülker, B., Somssich, I.E., and Schulze-Lefert, P. (2007). Nuclear activity of MLA immune receptors links isolate-specific and basal disease-resistance responses. Science *315*, 1098–1103. https://doi.org/10.1126/science.1136372.
87. Velásquez-Zapata, V., Elmore, J.M., Banerjee, S., Dorman, K.S., and Wise, R.P. (2021). Next-generation yeast-two-hybrid analysis with Y2H-SCORES identifies novel interactors of the MLA immune receptor. PLoS Comput. Biol. *17*, e1008890. https://doi.org/10.1371/journal.pcbi.1008890.
88. Chethana, K.W.T., Jayawardena, R.S., Chen, Y.J., Konta, S., Tibpromma, S., Abeywickrama, P.D., Gomdola, D., Balasuriya, A., Xu, J., Lumyong, S., and Hyde, K.D. (2021). Diversity and function of appressoria. Pathogens *10*, 746. https://doi.org/10.3390/pathogens10060746.
89. Lambertucci, S., Orman, K.M., Das Gupta, S., Fisher, J.P., Gazal, S., Williamson, R.J., Cramer, R., and Bindschedler, L.V. (2019). Analysis of barley leaf epidermis and extrahaustorial proteomes during powdery mildew infection reveals that the PR5 Thaumatin-like protein TLP5 is required for susceptibility towards *Blumeria graminis* f. sp. *hordei*. Front. Plant Sci. *10*, 1138. https://doi.org/10.3389/fpls.2019.01138.
90. Ahmed, A.A., Pedersen, C., and Thordal-Christensen, H. (2016). The barley powdery mildew effector candidates CSEP0081 and CSEP0254 promote fungal infection success. PLoS One *11*, e0157586. https://doi.org/10.1371/journal.pone.0157586.
91. Li, X., Jin, C., Yuan, H., Huang, W., Liu, F., Fan, R., Xie, J., and Shen, Q.-H. (2021). The barley powdery mildew effectors CSEP0139 and CSEP0182 suppress cell death and promote *B. graminis* fungal virulence in plants. Phytopathol. Res. *3*, 7. https://doi.org/10.1186/s42483-021-00084-z.
92. Pham, T.A.T., Schwerdt, J.G., Shirley, N.J., Xing, X., Hsieh, Y.S.Y., Srivastava, V., Bulone, V., and Little, A. (2019). Analysis of cell wall synthesis and metabolism during early germination of *Blumeria graminis* f. sp. *hordei* conidial cells induced in vitro. Cell Surf. *5*, 100030. https://doi.org/10.1016/j.tcsw.2019.100030.
93. Ellingboe, A.H. (1972). Genetics and physiology of primary infection by *Erysiphe graminis*. Phytopathology *62*, 401. https://doi.org/10.1094/Phyto-62-401.
94. Moscou, M.J., Lauter, N., Caldo, R.A., Nettleton, D., and Wise, R.P. (2011). Quantitative and temporal definition of the *Mla* transcriptional regulon during barley-powdery mildew interactions. Mol. Plant Microbe Interact. *24*, 694–705. https://doi.org/10.1094/MPMI-09-10-0211.
95. Caldo, R.A., Nettleton, D., and Wise, R.P. (2004). Interaction-dependent gene expression in *Mla*-specified response to barley powdery mildew. Plant Cell *16*, 2514–2528. https://doi.org/10.1105/tpc.104.023382.
96. Caldo, R.A., Nettleton, D., Peng, J., and Wise, R.P. (2006). Stage-specific suppression of basal defense discriminates barley plants containing fast- and delayed-acting *Mla* powdery mildew resistance alleles. Mol. Plant Microbe Interact. *19*, 939–947. https://doi.org/10.1094/MPMI-19-0939.
97. Barsoum, M., Kusch, S., Frantzeskakis, L., Schaffrath, U., and Panstruga, R. (2020). Ultraviolet mutagenesis coupled with next-generation sequencing as a method for functional interrogation of powdery mildew genomes. Mol. Plant Microbe Interact. *33*, 1008–1021. https://doi.org/10.1094/MPMI-02-20-0035-TA.
98. Bernasconi, Z., Stirnemann, U., Heuberger, M., Sotiropoulos, A.G., Graf, J., Wicker, T., Keller, B., and Sánchez-Martín, J. (2024). Mutagenesis of wheat powdery mildew reveals a single gene controlling both NLR and tandem kinase-mediated immunity. Mol. Plant Microbe Interact. *37*, 264–276. https://doi.org/10.1094/MPMI-09-23-0136-FI.
99. Moseman, J.G. (1972). Isogenic barley lines for reaction to *Erysiphe graminis* f. sp. *hordei*. Crop Sci. *12*, 681–682. https://doi.org/10.2135/cropsci1972.0011183X001200050038x.
100. Hemshrot, A., Poets, A.M., Tyagi, P., Lei, L., Carter, C.K., Hirsch, C.N., Li, L., Brown-Guedira, G., Morrell, P.L., Muehlbauer, G.J., and Smith, K.P. (2019). Development of a multiparent population for genetic mapping and allele discovery in six-row barley. Genetics *213*, 595–613. https://doi.org/10.1534/genetics.119.302046.
101. Yu, Y., Tomkins, J.P., Waugh, R., Frisch, D.A., Kudrna, D., Kleinhofs, A., Brueggeman, R.S., Muehlbauer, G.J., Wise, R.P., and Wing, R.A. (2000). A bacterial artificial chromosome library for barley (*Hordeum vulgare* L.) and the identification of clones containing

putative resistance genes. Theor. Appl. Genet. *101*, 1093–1099. https://doi.org/10.1007/s001220051584.

102. Love, M.I., Huber, W., and Anders, S. (2014). Moderated estimation of fold change and dispersion for RNA-seq data with DESeq2. Genome Biol. *15*, 550. https://doi.org/10.1186/s13059-014-0550-8.
103. RCoreTeam (2013). R: A language and environment for statistical computing.
104. Altschul, S.F., W, G., W, M., EW, M., and DJ, L. (1990). Basic local alignment search tool. J. Mol. Biol. *215*, 410.
105. Quinlan, A.R., and Hall, I.M. (2010). BEDTools: A flexible suite of utilities for comparing genomic features. Bioinformatics *26*, 841–842. https://doi.org/10.1093/bioinformatics/btq033.
106. Li, H., and Durbin, R. (2009). Fast and accurate short read alignment with Burrows–Wheeler transform. Bioinformatics *25*, 1754–1760. https://doi.org/10.1093/bioinformatics/btp324.
107. Robinson, J.T., Thorvaldsdóttir, H., Winckler, W., Guttman, M., Lander, E.S., Getz, G., and Mesirov, J.P. (2011). Integrative genomics viewer. Nat. Biotechnol. *29*, 24–26. https://doi.org/10.1038/nbt.1754.
108. Grabherr, M.G., Haas, B.J., Yassour, M., Levin, J.Z., Thompson, D.A., Amit, I., Adiconis, X., Fan, L., Raychowdhury, R., Zeng, Q., et al. (2011). Full-length transcriptome assembly from RNA-Seq data without a reference genome. Nat. Biotechnol. *29*, 644–652. https://doi.org/10.1038/nbt.1883.
109. Yu, G., Wang, L.-G., Han, Y., and He, Q.-Y. (2012). clusterProfiler: An R package for comparing biological themes among gene clusters. OMICS *16*, 284–287. https://doi.org/10.1089/omi.2011.0118.
110. Wickham, H. (2016). ggplot2: Elegant Graphics for Data Analysis (Springer-Verlag).
111. Lawrence, M., Huber, W., Pagès, H., Aboyoun, P., Carlson, M., Gentleman, R., Morgan, M.T., and Carey, V.J. (2013). Software for computing and annotating genomic ranges. PLoS Comput. Biol. *9*, 1–10. https://doi.org/10.1371/journal.pcbi.1003118.
112. Yin, T., Cook, D., and Lawrence, M. (2012). ggbio: an R package for extending the grammar of graphics for genomic data. Genome Biol. *13*, R77. https://doi.org/10.1186/gb-2012-13-8-r77.
113. Graves, S., Piepho, H.-P., Selzer, L., and Dorai-Raj, S. (2019). multcompView. Manual *1–24*. https://cran.r-project.org/web/packages/multcompView/multcompView.pdf.
114. Di Tommaso, P., Chatzou, M., Floden, E.W., Barja, P.P., Palumbo, E., and Notredame, C. (2017). Nextflow enables reproducible computational workflows. Nat. Biotechnol. *35*, 316–319. https://doi.org/10.1038/nbt.3820.
115. Ewels, P.A., Peltzer, A., Fillinger, S., Patel, H., Alneberg, J., Wilm, A., Garcia, M.U., Di Tommaso, P., and Nahnsen, S. (2020). The nf-core framework for community-curated bioinformatics pipelines. Nat. Biotechnol. *38*, 276–278. https://doi.org/10.1038/s41587-020-0439-x.
116. Patel, H., Ewels, P., Peltzer, A., Hammarén, R., Botvinnik, O., Sturm, G., Moreno, D., Vemuri, P., and Pantano, L. (2021). nf-core/rnaseq: nf-core/rnaseq v3.4 - Aluminium Aardvark. https://doi.org/10.5281/ZENODO.5550247.
117. Mascher, M., Wicker, T., Jenkins, J., Plott, C., Lux, T., Koh, C.S., Ens, J., Gundlach, H., Boston, L.B., Tulpová, Z., et al. (2021). Long-read sequence assembly: A technical evaluation in barley. Plant Cell *33*, 1888–1906. https://doi.org/10.1093/plcell/koab077.
118. Blake, V.C., Woodhouse, M.R., Lazo, G.R., Odell, S.G., Wight, C.P., Tinker, N.A., Wang, Y., Gu, Y.Q., Birkett, C.L., Jannink, J.L., et al. (2019). GrainGenes: Centralized small grain resources and digital platform for geneticists and breeders. Database *2019*, baz065. https://doi.org/10.1093/database/baz065.
119. Krueger, F. (2012). Trim Galore. https://www.bioinformatics.babraham.ac.uk/projects/trim_galore/.
120. Andrews, S. (2010). FastQC: A Quality Control Tool for High Throughput Sequence Data. http://www.bioinformatics.babraham.ac.uk/projects/fastqc/.
121. Martin, M. (2011). Cutadapt removes adapter sequences from high-throughput sequencing reads. EMBnet. j. *17*, 10–12. https://doi.org/10.14806/ej.17.1.200.
122. Dobin, A., Davis, C.A., Schlesinger, F., Drenkow, J., Zaleski, C., Jha, S., Batut, P., Chaisson, M., and Gingeras, T.R. (2013). STAR: ultrafast universal RNA-seq aligner. Bioinformatics *29*, 15–21. https://doi.org/10.1093/bioinformatics/bts635.
123. Patro, R., Duggal, G., Love, M.I., Irizarry, R.A., and Kingsford, C. (2017). Salmon provides fast and bias-aware quantification of transcript expression. Nat. Methods *14*, 417–419. https://doi.org/10.1038/nmeth.4197.
124. Klingenberg, H., and Meinicke, P. (2017). How to normalize metatranscriptomic count data for differential expression analysis. PeerJ *5*, e3859. https://doi.org/10.7717/peerj.3859.
125. Anders, S., and Huber, W. (2010). Differential expression analysis for sequence count data. Genome Biol. *11*, R106. https://doi.org/10.1186/gb-2010-11-10-r106.
126. Benjamini, Y., and Hochberg, Y. (1995). Controlling the false discovery rate: A practical and powerful approach to multiple testing. J. R. Stat. Soc. Ser. B *57*, 289–300. https://doi.org/10.1111/j.2517-6161.1995.tb02031.x.

STAR★METHODS

KEY RESOURCES TABLE

REAGENT or RESOURCE	SOURCE	IDENTIFIER
Experimental models: Organisms/strains		
Hordeum vulgare L.	C. I. (Cereal Introduction) 16151, Moseman 1972[99]	CI 16151
H. vulgare mutant line *mla6*	Kept in lab Chapman et al. 2021[43]	*mla6*-m18982
H. vulgare mutant line *bln1*	Kept in lab Chapman et al. 2021[43]	*bln1*-m19089
H. vulgare mutant line *mla6*, *bln1*	Kept in lab Chapman et al. 2021[43]	(*mla6* + *bln1*)-m19028
H. vulgare mutant line *sgt1* (*Sgt1*$_{\Delta KL308\text{-}309}$)	Kept in lab Chapman et al. 2021[43]	*rar3*-m11526
H. vulgare	University of Minnesota Hemshrot et al. 2019[100]	Rasmusson
H. vulgare	University of Minnesota; Hemshrot et al. 2019[100]	Clho15600
H. vulgare	Washington State University; Yu et al. 2000[101]	Morex
Blumeria hordei	Danish isolate kept in lab	5874 (*AVRa1*, *AVRa3*, *AVRa6*, *AVRa12*)
Blumeria hordei	U.K. isolate kept in lab	CC148 (*AVRa1*, *AVRa7*, *AVRa9*, *AVRa10*, *AVRa13*, *AVRa15*)
Psuedomonas syringae	Cornell University; Carter et al. 2019[74]	DC3000(D36E):AvrPphB
Reagents		
54% Phenol (equilibrated to pH 4.3)	Fisher	BP1751
1.43M Guanidine thiocyanate	Fisher	BP221-250
1.43M Ammonium thiocyanate	Fisher	A709-500
0.144M Sodium acetate (pH 5)	Fisher	BP333-500
0.07% Glycerol	Fisher	G33-500
Chloroform	Fisher	C298-4
Isopropanol	Fisher	BP2632-4
75% EtOH	Sigma	E7023-500
Recombinant Rnasin Ribonuclease Inhibitor	Promega	N2515
DNaseI	ThermoFisher	AM1906
RNeasy Plant Mini Kit	Qiagen	74904
CRITERION Protease Peptone No. 3	Hardy Diagnostics	Catalog #C6641
Magnesium sulfate heptahydrate	Sigma	Catalog # 63138
Potassium phosphate dibasic	Sigma	Catalog #P8281
Glycerol	Research Products International (RPI)	Catalog #G22025–0.5
Bacto Agar	Becton, Dickinson and Company (BD)	Catalog # BD214010
Rifampicin	Sigma	Catalog #R3501-1G
Kanamycin	Gibco	Catalog # 11815-032
Magnesium chloride	Fisher	Catalog #M35-500
Needless syringes	BD Slip Tip Sterile Syringes	Catalog # 14-823-434
Standard Round Planting Pots (11.43 cm × 10.16 cm)	Greenhouse Megastore	Catalog # CN-STD-0450

(*Continued on next page*)

Continued

REAGENT or RESOURCE	SOURCE	IDENTIFIER
Critical commercial assays		
TruSeq Stranded Total RNA Library Prep Gold (96 Samples)	Illumina	Cat#20020599
Software		
nf-core/rnaseq	Nextflow DSL2	https://nf-co.re/rnaseq/3.4.0
DESeq2	Love et al. 2014[102]	https://bioconductor.org/packages/release/bioc/html/DESeq2.html
R v4	The R project[103]	https://www.r-project.org/
Blast	Altschul SF et al. 1990[104]	https://anaconda.org/bioconda/blast
Bedtools	Quinlan and Hall 2010[105]	https://anaconda.org/bioconda/bedtools
BWA-mem	Li and Durbin 2009[106]	https://bioconda.github.io/recipes/bwa/README.html
IGV	Robinson et al. 2011[107]	https://igv.org/
Trinity	Grabherr et al. 2011[108]	https://bioconda.github.io/recipes/trinity/README.html
clusterProfiler	Yu et al. 2012[109]	https://bioconductor.org/packages/release/bioc/html/clusterProfiler.html
ggplot2	Wickham 2016[110]	https://ggplot2.tidyverse.org/
GenomicRanges	Lawrence et al. 2013[111]	https://bioconductor.org/packages/release/bioc/html/GenomicRanges.html
WGCNA	Langfelder and Horvath 2008[77]	https://cran.r-project.org/web/packages/WGCNA/index.html
Interproscan	Jones et al. 2014[78]	https://github.com/ebi-pf-team/interproscan
ggbio	Yin et al. 2012[112]	https://www.bioconductor.org/packages/release/bioc/html/ggbio.html
multcompView	Graves et al. 2019[113]	https://cran.r-project.org/web/packages/multcompView/index.html
Deposited data		
Morex V3 reference genome	USDA GrainGenes database	https://wheat.pw.usda.gov/GG3/content/morex-v3-files-2021
Bh DH14 genome assembly	Ensembl database	https://fungi.ensembl.org/Blumeria_graminis/Info/Index
RNA-Seq raw reads	GEO database	https://www.ncbi.nlm.nih.gov/geo/query/acc.cgi?acc=GSE101304

EXPERIMENTAL MODEL AND STUDY PARTICIPANT DETAILS

For each replication of this study, barley was planted in separate 19.5 × 27.5-cm trays using sterilized potting mix. Seedlings were grown in a climate-controlled greenhouse with both natural and artificial (HPS 400 bulbs) light using a randomized block design. Seven days after sowing, seedling trays were inoculated at 16:00 with a high density of *Bh* isolate 5874 (AVR_{a6}) and positioned randomly in a controlled growth chamber (18°C, 8 h darkness, 16 h light). Rows of seedlings were harvested at the assigned time points, pooled, and immediately placed into liquid nitrogen.

For the in planta infiltration assay, barley were sown in 4.5in (11.4 cm) plastic pots containing Berger Seed and Propagation Mix supplemented with Osmocote slow-release fertilizer (14-14-14) and maintained in a growth chamber with a 16:8 h photoperiod (light:dark) at 24°C with light and 20°C in the dark, with average light intensities at plant height of 120 μmols/m^2/s.

Blumeria hordei (*Bh*) isolates 5874 (AVR_{a1}, AVR_{a3}, AVR_{a6}, and AVR_{a12}) and CC148 (AVR_{a1}, AVR_{a7}, AVR_{a9}, AVR_{a10}, AVR_{a13}, and AVR_{a15}) were propagated on barley cv. Morex (C.I. 15773) in a Percival growth chamber (model PGC.15.5) at 18°C with a 16 h photoperiod (01:00 to 17:00 USA Central Standard Time). Light intensity at plant level was 120 μmol m2 s−1. Infection types were checked monthly via inoculation of a differential set with incompatible and compatible *Mla* alleles.

METHOD DETAILS

Transcriptome data collection

A temporal transcriptome of interacting host and pathogen was obtained from an infection time course of five barley genotypes with *Blumeria hordei* (*Bh*) isolate 5874 which carries the AVR_{a6} effector. The barley genotypes consisted of a resistant, wild-type plant (CI 16151) that carries the *Mla6* gene and four mutants derived by fast-neutron mutagenesis of the CI 16151 progenitor.[43] Plants that carry the *bln1* mutation (*bln1*-m19089) are resistant, while the other three are susceptible; an *mla6* mutant (*mla6*-m18982), a *sgt1* mutant (*rar3*-m11526 = $Sgt1_{\Delta KL308\text{-}309}$), and the double mutant (*mla6*+*bln1*)-m19028. The split-plot design contained 90 samples, comprised of 5 genotypes, 6 timepoints (0, 16, 20, 24, 32, and 48 HAI), and 3 independent biological replicates. First leaves were challenged with *Bh* isolate 5874[95] and then leaves were collected at each timepoint, for each genotype and replicate. RNA was extracted with hot (60°C) phenol/guanidine thiocyanate.[95,96] Libraries were prepared using the Illumina TruSeq stranded RNA sample preparation kit (Illumina, Inc., San Diego, CA) and sequenced with the Illumina HiSeq2500 system, using a randomized block design with single-end 100-bp reads (Figure S1).

Transcriptome profiling

We utilized the Nextflow DSL2[114] nf-core/rnaseq pipeline version 3.4[115,116] to align and quantify mRNA sequencing data from barley, *Hordeum vulgare* L., and *Bh*. The 90 RNA-Seq libraries were deposited to NCBI-GEO system, accession GSE101304. The reads were aligned and quantified against the *Bh* DH14 genome assembly (NCBI accession GCA_900239735.1) and annotation from the Ensembl database (https://fungi.ensembl.org/Blumeria_graminis/Info/Index) obtained from Stefan Kusch at RWTH Aachen University.[50] The pipeline for *Bh* was run with the additional parameters: "–skip_multiqc". Similarly, all RNA-Seq libraries were aligned against the barley Morex V3 reference genome and annotation[117] obtained from the USDA GrainGenes database.[118] The barley pipeline was run with the following parameters:

"–skip_multiqc –bam_csi_index –rseqc_modules 'bam_stat, infer_experiment,junction_annotation, junction_saturation,read_duplication'".

The pipeline consisted of adapter and quality trimming using Trim Galore,[119–121] read mapping with STAR[122] and quantification with Salmon.[123]

Differential expression analysis

Read counts were normalized using the taxon-specific method.[124] Each raw count table (barley and *Bh*) was taken and size factors calculated using median-of-ratios normalization.[125] Then, normalized tables were combined and used as input for DESeq2,[102] assigning the calculated size factors to the counts before calculating differentially expressed genes (DEGs). Continuing with the DESeq2 pipeline, DEGs were identified using a model with read counts as response variable, and timepoint*genotype terms as explanatory variables. Results from this analysis, including fold changes and *p*-values were taken for subsequent analyses. Adjusted *p*-values[126] were used to determine DEGs using <0.001 for barley and <0.003 for *Bh*.

Mutant characterization

Fast-neutron mutants of *Mla6* and *Bln1* were identified and distinguished by genetic complementation followed by differential expression, first by Affymetrix Barley1 GeneChip analysis,[65,66] and more recently, by RNA-Seq read mapping between wild-type progenitor and each single mutant (Figure S2). The *sgt1* mutation was previously characterized[43] as an in-frame Lys-Leu deletion in the SGS domain of Suppressor of the G2 allele of SKP1 ($Sgt1_{\Delta KL308\text{-}309}$). As outlined in,[43] susceptible mutant m11506, containing *mla6* and *bln1* mutations, was backcrossed and selfed twice to CI 16151 to select homozygous single mutants m18982 (*mla6*, *Bln1*, *Sgt1*), m19089 (*Mla6*, *bln1*, *Sgt1*), and double mutant m19028 (*mla6*, *bln1*, *Sgt1*). Similarly, *rar3*-m11526 (*Mla6*, *Bln1*, $Sgt1_{\Delta KL308\text{-}309}$), was made homozygous following two backcrosses to CI 16151 with selection.

To map the extent of the *mla6* and *bln1* mutations, several regions from the barley Morex V3 genome[117] were extracted as follows: 1) We analyzed *Mla* (HORVU.MOREX.r3.1HG0012670) and flanking genes in its proximity that had differential expression between the wild-type and the *mla6*-m18982 mutant; we also included all the genes in the *Mla* locus as reported by Wei and colleagues[19]; lastly, all the genes without mapped reads in *mla6*-m18982 were added to the list. 2) *Bln1* was not annotated in the Morex V3 assembly. To identify the *bln1* mutation, we used BLAST with the *Bln1* sequence (NCBI ID FJ156737.1) against the Morex V3 genome to identify its coordinates and then extracted differentially expressed genes between wild-type and *bln1*-m19089 mutant in the *Bln1* vicinity. In addition, we added all the genes without reads mapped in the *bln1*-m19089 mutant. To all these lists we added 1000 bp at the 5′ and 3′ ends.

The genomic coordinates were used to extract the corresponding sequences using bedtools.[105] After extracting the regions of the candidate genes, we mapped the RNA-Seq reads back to them from the wild-type, single and double mutants for the timepoints 16 and 20 HAI. We used BWA-mem[106] for mapping and IGV[107] for visualization. The bam files were used for a reference-guided assembly using Trinity.[108] We compared the mappings and assemblies to identify differences between wild-type progenitor and mutants. Consensus gene candidates across samples were analyzed to identify the effects of the mutations.

In planta infiltration assay

Pseudomonas syringae DC3000 D36E uniquely expressing the effector AvrPphB [*P. syringae* D36E (AvrPphB)] was generated in a previous study.[74] *P. syringae* D36E (AvrPphB) was cultured using King's B media supplemented with 50 μg/mL kanamycin and 50 μg/mL rifampicin for 2 days at 28°C. Bacteria were resuspended in 10 mM $MgCl_2$ to optical density (O.D.) at 600 nm (OD_{600}) of 0.5. Bacterial suspensions were syringe-infiltrated into the adaxial surface of the L2 leaf of 10-day-old barley. Three days following *Pseudomonas* infiltration, infiltrated

leaves were harvested and photographed under white light. Blind ratings were independently assessed by three individuals based on a predefined scale according to Carter and colleagues[74] encompassing no immune response (N; Morex), low chlorosis (LC; CI 16151, CIho15600), chlorosis (C), high chlorosis (HC), or hypersensitive reaction (HR; Rasmusson).

Gene effect models

We designed two methods for evaluating the gene effects of the *Mla6, Bln1* and *Sgt1* genes.

Model Mla6, Bln1

The first model (*Mla6, Bln1*) is a full epistasis design as we had data from single and double mutants. Let E(G) be the log of the global gene expression levels of a plant with the genotype G. For analyzing the effects of the pair *Mla6, Bln1* we write the global expression equation for each genotype. If *DB* is defined as the Defense Background genotype, the collection of genes in G involved in defense responses and common to all the genotypes:

$$E(Mla6, Bln1) = Mla6 + Bln1 + Mla6 * Bln1 + Mla6 * DB + Bln1 * DB + DB$$

$$E(Mla6, bln1) = Mla6 + Mla6 * bln1 + Mla6 * DB + DB = Mla6 + Mla6 * DB + DB$$

$$E(mla6, Bln1) = Bln1 + Bln1 * DB + DB$$

$$E(mla6, bln1) = DB$$

We can calculate differentially expressed genes among a pair of genotypes (DEG(G1/G2)) as the difference between their expression E(G1) – E(G2). For example, DEGs between CI 16151 (WT) and each of the mutants:

$$DEG(Mla6, Bln1 \,/\, Mla6, bln1) = E(Mla6, Bln1) - E(Mla6, bln1) = Mla6 + Bln1 + Mla6 * Bln1 + Mla6 * DB + Bln1 * DB + DB - (Mla6 + Mla6 * DB + DB)$$

$$= Bln1 + Mla6 * Bln1 + Bln1 * DB$$

$$DEG(Mla6, Bln1 \,/\, mla6, Bln1) = E(Mla6, Bln1) - E(mla6, Bln1) = Mla6 + Bln1 + Mla6 * Bln1 + Mla6 * DB + Bln1 * DB + DB - (Bln1 + Bln1 * DB + DB)$$

$$= Mla6 + Mla6 * Bln1 + Mla6 * DB$$

$$DEG(Mla6, Bln1 \,/\, mla6, bln1) = Mla6 + Bln1 + Mla6 * Bln1 + Mla6 * DB + Bln1 * DB + DB - (DB) = Mla6 + Bln1 + Mla6 * Bln1 + Mla6 * DB + Bln1 * DB$$

And with the double mutant as reference:

$$DEG(Mla6, bln1 \,/\, mla6, bln1) = Mla6 + Mla6 * DB$$

$$DEG(mla6, Bln1 \,/\, mla6, bln1) = Bln1 + Bln1 * DB$$

$$DEG(Mla6, Bln1 \,/\, mla6, bln1) = Mla6 + Bln1 + Mla6 * Bln1 + Mla6 * DB + Bln1 * DB$$

We assigned DEG() = 0 as a fold change equal to zero, i.e., there are no significant differences. DEG()≠0 means there are significant differences and considering all values of the *p*-value and fold change. DEG()>0, DEG()<0 indicate significant differences and the sign of the fold change in the comparison. To declare a significant difference a p-adjusted value of 0.001 was applied. Additionally, a change in the fold change proportion in the top 20% of the significant differences based on p-adjusted was considered epistatic. Genes whose expression deviated from the expected value were classified as epistatic while the ones that fitted the expected value were considered additive.

1) Epistatic effects, Epi(*Mla6, Bln1*):

DEG(*Mla6, Bln1/mla6, bln1*) – DEG(*Mla6, Bln1/mla6, Bln1*) – DEG(*Mla6, Bln1/Mla6, bln1*)≠*0*

$$= Mla6 + Bln1 + Mla6 * Bln1 + Mla6 * DB + Bln1 * DB - (Mla6 + Mla6 * Bln1 + Mla6 * DB + Bln1 + Mla6 * Bln1 + Bln1 * DB) \neq 0 \rightarrow Mla6 * Bln1 \neq 0$$

2) No epistasis, additive effects of *Mla6* and *Bln1*, Addi(*Mla6*, *Bln1*):

$$\mathrm{DEG(Mla6, Bln1\ /\ mla6, bln1)} - \mathrm{DEG(Mla6, Bln1\ /\ mla6, Bln1)} - \mathrm{DEG(Mla6, Bln1\ /\ Mla6, bln1)} = 0$$

$$\rightarrow \mathrm{Mla6} * \mathrm{Bln1} = 0$$

Epistatic genes were further classified in five categories and by comparing each single mutant to the double mutant. First, genes under symmetric epistasis were calculated as those which have no significant differences between each single mutant and the double mutant, which implies that *Mla6* and *Bln1* have the same effects on the gene expression. Masked epistasis (*Mla6* counteracts the effect of *Bln1*) was defined for those genes where there were no significant differences between the mla6 mutant and the double mutant but the comparison between the bln1 mutant and the double mutant was significant. Similarly, suppression epistasis (*Bln1* counteracts the effect of *Mla6*) was calculated for those whose expression is the same between the *bln1* and the double mutant, while different between the mla6 and the double mutant.

3) Symmetric epistasis:

$\mathrm{Epi}(Mla6, Bln1) \cap [\mathrm{DEG}(Mla6, bln1/mla6, bln1) = 0 \cap \mathrm{DEG}(mla6, Bln1/mla6, bln1) = 0]$

$$= \mathrm{Mla6} * \mathrm{Bln1} \neq 0, \mathrm{Mla6} + \mathrm{Mla6} * \mathrm{DB} = 0, \mathrm{Bln1} + \mathrm{Bln1} * \mathrm{DB} = 0$$

$$\rightarrow \mathrm{Mla6} * \mathrm{Bln1} \neq 0 \ \mathrm{AND}\ \mathrm{Mla6} + \mathrm{Mla6} * \mathrm{DB} = \mathrm{Bln1} + \mathrm{Bln1} * \mathrm{DB}$$

4) Masked epistasis:

$\mathrm{Epi}(Mla6, Bln1) \cap [\mathrm{DEG}(Mla6, bln1/mla6, bln1) \neq 0 \cap \mathrm{DEG}(mla6, Bln1/mla6, bln1) = 0]$

$$= \mathrm{Mla6} * \mathrm{Bln1} \neq 0, \mathrm{Mla6} + \mathrm{Mla6} * \mathrm{DB} \neq 0, \mathrm{Bln1} + \mathrm{Bln1} * \mathrm{DB} = 0$$

$$\rightarrow \mathrm{Mla6} * \mathrm{Bln1} \neq 0 \ \mathrm{AND}\ \mathrm{Mla6} + \mathrm{Mla6} * \mathrm{DB} \neq 0$$

5) Suppression epistasis:

$$\mathrm{Epi(Mla6, Bln1)} \cap [\mathrm{DEG(Mla6, bln1\ /\ mla6, bln1)} = 0 \cap \mathrm{DEG(mla6, Bln1\ /\ mla6, bln1)} \neq 0]$$

$$= \mathrm{Mla6} * \mathrm{Bln1} \neq 0, \mathrm{Mla6} + \mathrm{Mla6} * \mathrm{DB} = 0, \mathrm{Bln1} + \mathrm{Bln1} * \mathrm{DB} \neq 0$$

$$\rightarrow \mathrm{Mla6} * \mathrm{Bln1} \neq 0 \ \mathrm{AND}\ \mathrm{Bln1} + \mathrm{Bln1} * \mathrm{DB} \neq 0$$

The next set of patterns include pseudo masked, positive and negative epistasis. Pseudo masked epistasis was calculated for the genes whose expression in the double mutant was between the *mla6* and the *bln1* mutant. There are two scenarios where this is fulfilled, either when the expression is higher in the bln1 mutant and lower in the mla6 mutant or vice versa. In positive epistasis, the expression of the single mutants is less than the observed in the double mutants, while in negative epistasis the double mutant expression is less than for any on the single mutants.

6) Pseudo Masked epistasis:

$$\mathrm{Epi(Mla6, Bln1)} \cap [\mathrm{DEG(Mla6, bln1\ /\ mla6, bln1)} > 0 \cap \mathrm{DEG(mla6, Bln1\ /\ mla6, bln1)} < 0]$$

$$\rightarrow \mathrm{Mla6} * \mathrm{Bln1} \neq 0 \ \mathrm{AND}\ \mathrm{Mla6} + \mathrm{Mla6} * \mathrm{DB} > 0 \ \mathrm{AND}\ \mathrm{Bln1} + \mathrm{Bln1} * \mathrm{DB} < 0$$

OR

$$\mathrm{Epi(Mla6, Bln1)} \cap [\mathrm{DEG(Mla6, bln1\ /\ mla6, bln1)} < 0 \cap \mathrm{DEG(mla6, Bln1\ /\ mla6, bln1)} > 0]$$

$$\rightarrow \mathrm{Mla6} * \mathrm{Bln1} \neq 0 \ \mathrm{AND}\ \mathrm{Mla6} + \mathrm{Mla6} * \mathrm{DB} < 0 \ \mathrm{AND}\ \mathrm{Bln1} + \mathrm{Bln1} * \mathrm{DB} > 0$$

7) Positive epistasis:

$$Epi(Mla6, Bln1) \cap [DEG(Mla6, bln1\ /\ mla6, bln1)\ <\ 0 \cap DEG(mla6, Bln1 / mla6, bln1)\ <\ 0]$$

$$\rightarrow Mla6 * Bln1 \neq 0\ AND\ Mla6 + Mla6 * DB\ <\ 0\ AND\ Bln1 + Bln1 * DB\ <\ 0$$

8) Negative epistasis:

$$Epi(Mla6, Bln1) \cap [DEG(Mla6, bln1 / mla6, bln1)\ >\ 0 \cap DEG(mla6, Bln1\ /\ mla6, bln1)\ >\ 0]$$

$$\rightarrow Mla6 * Bln1 \neq 0\ AND\ Mla6 + Mla6 * DB\ >\ 0\ AND\ Bln1 + Bln1 * DB\ >\ 0$$

Model Mla6, Sgt1

The second model (*Mla6, Sgt1*) was defined taking the wild-type expression as reference, since the double mutant was not available. The model starts with the definition of the global gene expression and the differentially expressed gene effects:

$$E(WT)\ =\ E(Mla6, Sgt1) = Mla6 + Sgt1 + Mla6 * Sgt1 + Mla6 * DB + Sgt1 * DB + DB$$

$$E(Mla6, Sgt1\Delta KL308 - 309)\ =\ Mla6 + Mla6 * DB + DB$$

$$E(mla6, Sgt1)\ =\ Sgt1 + Sgt1 * DB + DB$$

Followed by the differentially expressed genes:

$$DEG(Mla6, Sgt1 / Mla6, Sgt1\Delta KL308 - 309)\ =\ Mla6 + Sgt1 + Mla6 * Sgt1 + Mla6 * DB + Sgt1 * DB + DB$$

$$- (Mla6 + Mla6 * DB + DB) = Sgt1 + Mla6 * Sgt1 + Sgt1 * DB$$

$$DEG(Mla6, Sgt1 / mla6, Sgt1)\ =\ Mla6 + Sgt1 + Mla6 * Sgt1 + Mla6 * DB + Sgt1 * DB + DB$$

$$- (Sgt1 + Sgt1 * DB + DB) = Mla6 + Mla6 * Sgt1 + Mla6 * DB$$

$$DEG(mla6, Sgt1\ /\ Mla6, Sgt1\Delta KL308 - 309)\ =\ Sgt1 + Sgt1 * DB + DB\ -\ (Mla6 + Mla6 * DB + DB)$$

$$= Sgt1 - Mla6 + Sgt1 * DB - Mla6 * DB$$

This model consisted in separating the gene effects by comparing the DEG lists from the comparison of the *mla6* and *sgt1* ($Sgt1_{\Delta KL308\text{-}309}$) single mutants with CI 16151 (WT). The intersection DEG(*Mla6, Sgt1*/*Mla6, sgt1*) ∩ DEG(*Mla6, Sgt1*/*mla6, Sgt1*) contains the shared effects between *Mla6* and *Sgt1*. Then, the difference between the DEG of each wild-type and mutant comparison contains the dominant effects of each gene.

1) Shared effects between *Mla6* and *Sgt1:* Shared(*Mla6, Sgt1*)=

$$DEG(Mla6, Sgt1 / Mla6, Sgt1_{\Delta KL308 - 309}) \neq 0 \cap DEG(Mla6, Sgt1 / mla6, Sgt1) \neq 0$$

$$\rightarrow Sgt1 + Mla6 * Sgt1 + Sgt1 * DB \neq 0\ AND\ Mla6 + Mla6 * Sgt1 + Mla6 * DB \neq 0$$

2) Dominant effects of *Sgt1:*

$$Dom(Sgt1)\ =\ [DEG(Mla6, Sgt1 / Mla6, sgt1) \neq 0] - Shared(Mla6, Sgt1)$$

$$\rightarrow Sgt1 + Mla6 * Sgt1 + Sgt1 * DB \neq 0\ AND\ Mla6 + Mla6 * Sgt1 + Mla6 * DB\ =\ 0$$

3) Dominant effects of *Mla6:*

$$\mathrm{Dom(Mla6)} = [\mathrm{DEG(Mla6, Sgt1 / mla6, Sgt1)} \neq 0] - \mathrm{Shared(Mla6, Sgt1)}$$

$$\rightarrow \mathrm{Mla6} + \mathrm{Mla6} * \mathrm{Sgt1} + \mathrm{Mla6} * \mathrm{DB} \neq 0 \ \mathrm{AND} \ \mathrm{Sgt1} + \mathrm{Mla6} * \mathrm{Sgt1} + \mathrm{Sgt1} * \mathrm{DB} = 0$$

This intersection DEG(*Mla6, Sgt1/Mla6, Sgt1*$_{\Delta KL308\text{-}309}$) ∩ DEG(*Mla6, Sgt1/mla6, Sgt1*) can be split in the genes that have an equal effect between the two mutants (with the same fold-change and no significant differences when they are compared), or predominant effects when the wild-type version of each gene (*Mla6* or *Sgt1*) has a greater effect on gene expression.

4) Equal effects between *Mla6* and *Sgt1:*

$$\mathrm{Equal(Mla6, Sgt1)} = \mathrm{Shared(Mla6, Sgt1)} \cap [\mathrm{DEG(mla6, Sgt1 / Mla6, Sgt1}_{\Delta \mathrm{KL308-309}}) = 0]$$

$$\rightarrow \mathrm{Mla6} + \mathrm{Mla6} * \mathrm{DB} = \mathrm{Sgt1} + \mathrm{Sgt1} * \mathrm{DB}$$

5) Predominant effects of *Sgt1:*

$$\mathrm{PreDom(Sgt1)} = \mathrm{Shared(Mla6, Sgt1)} \cap [\mathrm{DEG(mla6, Sgt1 / Mla6, Sgt1}_{\Delta \mathrm{KL308-309}}) > 0]$$

$$\rightarrow \mathrm{Mla6} + \mathrm{Mla6} * \mathrm{DB} < \mathrm{Sgt1} + \mathrm{Sgt1} * \mathrm{DB}$$

6) Predominant effects of *Mla6:*

$$\mathrm{PreDom(Mla6)} = \mathrm{Shared(Mla6, Sgt1)} \cap [\mathrm{DEG(mla6, Sgt1 / Mla6, Sgt1}_{\Delta \mathrm{KL308-309}}) < 0]$$

$$\rightarrow \mathrm{Mla6} + \mathrm{Mla6} * \mathrm{DB} > \mathrm{Sgt1} + \mathrm{Sgt1} * \mathrm{DB}$$

Bh infection kinetics

Data including microscopic quantification of fungal structures was obtained from Chapman et al.[43] Quantified structures included attached conidiospores, appressorial attachment, and hyphal indices 1, 2 and 3. Ten-centimeter (cm) seedlings for the timepoints 16, 20, 24, 32 and 48 HAI were assayed in triplicate. After inoculation with *Bh* 5874, five leaves assigned to each timepoint were harvested and submerged in clearing solution (3:1, alcohol: acetic acid) for at least 24 h and then transferred to 70% ethanol for another 24 h and then to 20% ethanol. Scoring was performed by treating the leaves with Coomassie blue for 2 min to visualize spores and hyphae. After staining, leaves were trimmed to 5 cm from the tip and structures were counted on both the abaxial and adaxial sides (Table S4).

QUANTIFICATION AND STATISTICAL ANALYSIS

Differential expression analysis

Read counts were normalized using the taxon-specific method.[124] Each raw count table (barley and *Bh*) was taken and size factors calculated using median-of-ratios normalization.[125] Then, normalized tables were combined and used as input for DESeq2,[102] assigning the calculated size factors to the counts before calculating differentially expressed genes (DEGs). Continuing with the DESeq2 pipeline, DEGs were identified using a model with read counts as response variable, and timepoint*genotype terms as explanatory variables. Results from this analysis, including fold changes and *p*-values were taken for subsequent analyses. Adjusted *p*-values[126] were used to determine DEGs using <0.001 for barley and <0.003 for *Bh*. Significant differences in figures with time-course expression graphs are designated by lower case letters (a,b,c).

GO analysis

Genes classified under each gene effect model and per timepoint and their consensus were analyzed using GO enrichment. Using clusterProfiler[109] and the GO terms reported for the barley and *Bh* annotations[50,117] we calculated gene enrichment with a *p*-value threshold of 0.05. We used ggplot2[110] to graph the functions of the genes under each pattern over time.

Chromosomal position analysis

Gene lists under the consensus of each gene effect classification model were used to perform genomic position analysis. Using GenomicRanges,[111] we binned the genes in the barley genome and then we designed a hypergeometric test to look for regions in the

genome with enrichment in each gene list. Taking genome windows of 1 Mb, 10 Mb, 100 Mb and the complete chromosome or scaffold we tested for enrichment of genes classified in each of the categories for each model, by considering the gene density in each bin as the reference for the test. We then adjusted the *p*-values using the Benjamini and Hochberg method[126] and considered significant enrichment using a threshold of 0.05. Barley genes that were classified in each pattern were plotted for the significant regions using the ggbio package.[112] Morex V3 centromere coordinates (Chr1H 206486643, Chr2H 301293086, Chr3H 267852507, Chr4H 276149121, Chr5H 204878572, Chr6H 256319444, and Chr7H 328847192) were used for reference as reported in.[70]

Comparison between genetic and protein interaction networks

Genes classified under each category of the *Mla6*, *Bln1* and *Mla6*, *Sgt1* models were compared with protein interaction networks described in Velásquez-Zapata et al.[73] For each category, a hypergeometric test was performed for the barley predicted interactome (HvInt), the MLA-associated interactome (MLAInt), the resistant and susceptible coexpressed interactomes and their difference [HvInt(R), HvInt(S) and HvInt(R-S)]. Significant enrichment was calculated with p-value<0.05.

Nucleotide-binding leucine-rich repeat (NLR) pattern analysis

The Morex V3 genome-wide barley NLR list[28] was taken to study the gene effects of *Mla6*, *Bln1* and *Sgt1*. Gene expression was clustered and a heatmap constructed for each group adding two layers of color annotations (one for each gene effect model). Gene expression patterns for each gene were also generated, calculating significant differences across time for each genotype comparison. These results were summarized using the package multcompView,[113] and using a letter code to show differences. Patterns were manually curated, and examples shown to characterize the dataset for each of the gene effect models. All NLR time-course expression graphs for CI 16151 progenitor and fast-neutron derived mutants are provided in Data S1.

Co-expression analysis

Bh normalized gene counts using DESeq2[102] were taken for all the replicates, genotypes and timepoints. Genes with complete gene counts were used to build the co-expression network by following the tutorials presented in the Weighted Gene Co-expression Network Analysis (WGCNA) R package.[77] The clustering was checked for quality and then co-expression clusters were calculated. To characterize these clusters functionally, we performed GO analysis using a hypergeometric test. GO annotations were obtained using Interproscan[78] and functional annotation for the *Bh* genome.[49,50] GO analysis was performed for the *Bh* co-expression clusters and enrichment terms (adjusted p-value <0.05) were reported.

The co-expression network was correlated with different phenotype traits including timepoint, disease phenotype and the infection kinetic structures. Significant associations were calculated at the cluster and gene level. Significant associations were characterized by GO analysis. In the case of effectors, a further functional table was obtained to perform the hypergeometric tests.[49]